Environmental Science and Pollution Research
https://doi.org/10.1007/s11356-024-32182-8

RESEARCH ARTICLE

Graphite/carbon-doped TiO_2 nanocomposite synthesized by ultrasound for the degradation of diclofenac

Mohammad Barjasteh Moghaddam Roshtkhari[1] · Mohammad Hassan Entezari[1,2]

Received: 22 July 2023 / Accepted: 21 January 2024

Abstract

Graphite/C-doped TiO_2 nanocomposite was synthesized at room temperature using a simple, impressive, and indirect sonication (20 kHz) by the cup horn system. Tetrabutyltitanate as the precursor of titanium and graphite (G) as the carbon source was used in the preparation of nanocomposite as a photocatalyst. The molar ratio of G/TiO_2 as a key parameter was investigated in the synthesis of G/C-doped TiO_2. The obtained materials were widely characterized using XRD, SEM, TEM, FTIR, XPS, and UV–Vis diffuse reflectance techniques. The UV–Vis diffuse reflectance spectroscopy results showed that the edge of light absorption of nanocomposite was distinctly red-shifted to the visible area via carbon doping. The XPS outcomes acknowledged the existence of the C, Ti, and O in the photocatalyst. The composite showed an enhancement in the dissociation efficiency of photoinduced charge carriers through the doping process. The photocatalytic activity of the synthesized nanocomposite was checked with diclofenac (DCF) as a pharmaceutical contaminant. The results displayed that G/C-doped TiO_2 represented better photocatalytic performance for DCF than TiO_2. This was due to the excellent crystallization, intense absorption of visible light, and the impressive separation of photoinduced charge carriers. Various active species such as $^{\bullet}OH$, $^{\bullet}O_2^-$, h^+, and H_2O_2 play a role in the degradation of DFC. Therefore, different scavengers were used and the role of each one in degradation was investigated. According to the obtained results, $^{\bullet}O_2^-$ radical showed a major role in the photocatalytic process. This work not only proposes a deep insight into the photosensitization-like mechanism by using G-based materials but also develops new photocatalysts for the removal of emerging organic pollutants from waters using sunlight as available cheap energy.

Keywords Ultrasound · Graphite · C-doped TiO_2 nanoparticles · Photocatalytic degradation · Diclofenac

Introduction

Water contamination has become a main problem in recent years. DCF is an anti-inflammatory and analgesic drug. It is often considered an emerging pollutant and is found in soil and drinking water. Studies have shown strong evidence of its serious risks to mammals, including humans (Velempini et al. 2021). Even in low concentrations, DCF can cause digestive, kidney, liver, blood, genetic, and even skin sensitivity complications. This drug was first developed in 1973 by Ciba-Geigy (Rozman et al. 2015). Considering that heart diseases are increasing due to the increase in the elderly population and the need for pain relief, therefore, consumption of 2400 tons of DCF has been reported in the world. Also, in 2020–2025, the DCF market is expected to achieve a growth rate of 3.87% and a revenue of $5.64 billion (Sathishkumar et al. 2021). Long-term exposure has been shown to negatively impact ecosystem health and sustainability. In addition, the formation of intermediate products during DCF degradation deserves more attention due to their complex and toxic natures. The detection accuracy level of DCF is owing to its retention in the natural aqueous environment, yet typical water treatment processes have little ability to effectively remove it. To destroy DCF, a few biological methods

Responsible Editor: Sami Rtimi

✉ Mohammad Hassan Entezari
entezari@um.ac.ir; moh_entezari@yahoo.com

[1] Sonochemical Research Center, Department of Chemistry, Faculty of Science, Ferdowsi University of Mashhad, Mashhad, Iran

[2] Environmental Chemistry Research Center, Department of Chemistry, Faculty of Science, Ferdowsi University of Mashhad, Mashhad, Iran

Published online: 30 January 2024

and advanced oxidation processes (AOPs) have been used (Li et al. 2020a). Since, some transitional biological, physical, and chemical methods have some limitations (transfer organic compounds to the solid phase and cause secondary water pollution, expensive operations regeneration of the adsorbent materials, and post-treatment of solid wastes) when they are used for DCF removal, AOPs can be an effective alternative (De Luis et al. 2011; Gümüş and Akbal 2011). The use of semi-conducting heterogeneous photocatalysts such as TiO_2, ZnO, and WO_3 is a promising and effective way to remove contaminants (Lara-Pérez et al. 2020; Nguyen and Nguyen 2020). In addition, they are prominent among the advanced oxidation processes (AOPs) as a powerful method for air and water purification (Malato et al. 2009; Binas et al. 2017). TiO_2 is one of the semiconductors that have been used as a diverse substance over the past decades, with its unique advantages, such as non-toxic, abundance in nature, strong photo-oxidizing power, and stability (Liu and Chen 2014). Studies have shown that the efficiency of TiO_2 photocatalytic activity is strongly dependent on the type of selective synthesis method, the corresponding phase purity, the efficiency of metal-free TiO_2 nanoparticles, and the excellent specific surface area (Byranvand et al. 2013; Kumar 2018). With these descriptions, numerous techniques like the sol–gel, hydrothermal, microwave, microemulsion, solvothermal, precipitation, and other methods have been confirmed to be effective and well organized (González-Reyes et al. 2010; Huang et al. 2013b). However, the practical use of TiO_2 as a photocatalyst is limited in the treatment of wastewater pollutants due to multiple dilemmas. Firstly, TiO_2 can only absorb UV light, which contains about 4% of the sun's light, owing to its wide band gap (3.2 eV) (Wang et al. 2013; Tseng and Chao 2013; Ong et al. 2014). Secondly, the great recombination rate of photoexcited charge carriers (e^-/h^+) decreased the quantum yield of TiO_2 (Cheng et al. 2012; Di et al. 2015). Thirdly, the separation and recycling of pulverous TiO_2 from the suspension system was a hard task (Cheng et al. 2013; Li et al. 2015b). Afterward, to overcome these defects, numerous methods have been tried to improve the optical response of TiO_2 from the UV into the visible light area. This has been done through doping TiO_2 with transition metals and the main group elements such as carbon, nitrogen, and sulfur (Cheng et al. 2012; Liu et al. 2013). In addition, coupling with other semiconductors with different band gaps (Kohtani et al. 1993) is another way of improving the optical response of TiO_2. Especially, the combination of TiO_2 nanomaterials with activated carbon (Baek et al. 2013), carbon nanotubes (Mohamed and Mkhalid 2015), graphene (Ullah et al. 2014), graphite (Jia et al. 2016) lately attracted notable consideration and demonstrated potential benefits over other kinds of modification techniques. These compounds have the following specific characteristics: (a) materials with C-source are used as electronic substances and have conductance like metals (Woan et al. 2009; Zhang et al. 2015a); (b) carbon materials have a large electron acceptance capacity and inhibit electron–hole (e^-/h^+) pair recombination (Kongkanand and Kama 2007; Zhang et al. 2013); (c) the thermal energy accumulated due to the absorption of visible light by carbon materials causes the movement of excited electrons from the mass of TiO_2 toward the reaction sites and improves the desired reaction by creating high-energy spaces (Lee et al. 2013; He et al. 2014); and (d) the carbon element can be transferred to the TiO_2 lattice by substituting some atoms and creating a C = O or C–O bond in the carbon doping process, which creates a hybrid just below the TiO_2 conductivity level and increases the performance in the visible region (Amalraj Appavoo et al. 2014; Li et al. 2015b). Graphite (G) as a carbon material has attracted much consideration due to its interesting features such as cost-effectiveness, availability, excellent-temperature resistance, compatibility, and production on a general large scale (Palmisano et al. 2009). G is a material with high stability and low density, which can be easily transformed due to its soft nature (Rajeshkumar et al. 2017). Over the last few years, ultrasound has had a more promising and important application in a diverse range of materials and chemical synthesis methods for the fabrication and modification of nanosized inorganic materials (Zhou et al. 2006; Bang and Suslick 2010). Ultrasound due to the physical and chemical effects caused by acoustic cavitation (formation, growth, and collapse of bubbles in a liquid) can be applied as a special method for producing new materials with unusual properties (Wang et al. 2012b; Colmenares 2013). A temperature of about 1000 K pressure of about 5000 atm and a cooling rate above 10^9 K/s can be caused by the explosion of bubbles (Sander et al. 2014). A bubble explosion causes shock waves in the liquid. These shock waves can both cause mass transfer and accelerate the solid particles suspended in the liquid. The solid particles suspended in the liquid due to the strong collisions cause the fragmentation of the fragile particles in the liquid, the exfoliation of layered materials, and the accumulation of materials that have the property of hammering. Also, when the bubble collapse is done asymmetrically, it causes the formation of high-speed micro-jets near the surface, which cause surface corrosion, material deformation, and pitting (Sander et al. 2014; Meroni et al. 2022; Mergbi et al. 2023). These critical conditions led to chemical reactions, new physical changes, and multiple nanostructured materials in different substances such as metals, alloys, oxides, and bio-substances (Safarifard and Morsali 2012). To improve the photocatalytic properties and the performance of TiO_2, the application and use of

ultrasound as a simple and practical method to change the band gap of TiO_2 by introducing specific elements have become a serious challenge (Tiple et al. 2021; da Silva et al. 2022). Compared to other methods, the use of ultrasonic waves reduces additional substances or mixtures in the synthesis reactions. Also, it is safe in the environment, easy to work, and relatively cheap (Shchukin et al. 2011). Moreover, this procedure reduces synthesis time, controls morphology, and further enhances non-metallic doping performance (Zhou et al. 2013).

In the literature, not many organized efforts can be found on the influence of ultrasound on the activity of nonmetal-doped TiO_2 (Teh et al. 2015). J. Jia et al. reported the fabrication of G/C-doped TiO_2 through a modified sol–gel and their highly efficient photocatalytic activity for methyl orange (MO) degradation (Jia et al. 2016). Therefore, as far as we know, there are not any reports in the literature on the synthesis of G/C-doped TiO_2 photocatalysts through the sonochemical procedure and there is no research on its photocatalytic results regarding the degradation of diclophenac. Herein, the synthesis of G/C-doped TiO_2 nanophotocatalyst was investigated at room temperature through an easy sonochemical method. Under these conditions, the coupling of graphite and the introduction of C-impurity into the TiO_2 lattice were carried out to improve its performance in the visible region. The sonosynthesis of G/C-doped TiO_2 nanophotocatalyst showed great efficiency in the decay of DCF in a short time. In the present work, we intend to show how a pure TiO_2 system can be easily sensitized to the xenon light via carbon doping and how practical aspects of both the material preparation (namely, the chemical nature of the dopant) and the conditions of the photocatalytic tests can affect the photoactivity results. The underlying mechanism of photocatalytic degradation of organic with specific structures by G-based photocatalyst was also fully discussed, which is of great importance to better understanding the key reactions in different photocatalysis systems. This study deals with applying ultrasonic treatment during the synthesis method to lower the particle size and enhance surface morphologies. The effect of pH and the photostability of the photocatalyst were also investigated.

Experimental section

Materials

The following chemical materials were purchased from their relevant suppliers and used without further purification. Tetra n-butyl orthotitanate (≥ 98%, Merk KGaA, 64271 Darmstadt) and ethanol (absolute, Fisher) were used for the synthesis of catalysts. Powder G, p-benzoquinone (BQ), HNO_3, NaOH from Merck, and DCF sodium ($C_{14}H_{10}Cl_2NNaO_2$) were from Sigma-Aldrich. In all experiments, Milli-Q water was used.

Synthesis of G/C-doped TiO_2 nanocomposite

G/C-doped TiO_2 was synthesized via sonication of the ethyl alcohol mixture of tetra n-butyl orthotitanate. In the synthesis, 10 mL of tetra-butyl orthotitanate was added dropwise to the 40 mL of absolute alcohol. It was stirred for 10 min at room temperature and the obtained homogeneous solution was called solution A. Solution B was prepared by a mixture of 12 mL of diluted nitric acid (by a volume ratio of 1:5 between nitric acid and deionized water) and 10 mL of absolute ethyl alcohol. Solution A was continuously sonicated for 10 min at 25 °C during the dropwise addition of solution B, and the final solution was called solution C. The reaction was performed under temperature control by a circulator. Then, G powder (0.03 g) was added to solution C and the black sol was continually sonicated for another 10 min. At the end of the sonication, the black sol remained in the laboratory for 24 h and then dried in an oven at 80 °C for 48 h. The obtained sample was ground in a porcelain mortar and calcined in a furnace at 350 °C for 2 h. The final composite was the nanocrystalline G/C-doped TiO_2. The other three samples were synthesized with 0.01, 0.05, and 0.10 g of G under similar conditions as the sample 0.03 g. The molar ratio of G/TiO_2 was calculated for 0.01, 0.03, 0.05, and 0.10 g of G (graphite) as 0.0284, 0.0852, 0.1418, and 0.2837, respectively. TiO_2 was also synthesized in the absence of G by the same method. All experiments were repeated at least three times and averages were reported. The schematic of the synthesis process of G/C-doped TiO_2 composite is shown in Fig. 1. To compare the sono-synthesis performance, the optimal sample was also synthesized by the sol–gel method. A cup horn (Fig. 1) offers indirect sonication and functions as a high-intensity ultrasonic water bath. Samples can be processed in sealed tubes or vials eliminating aerosols and cross contamination. Cup horns are ideal for sterile or pathogenic sample processing, and can be used to process samples too small for probe-style horns. The horn is mounted within a glass cup and the cup is filled with water. A sample tube is placed in the water reservoir above the horn. Cavitation is produced in the water, processing the sample within the tube. Sonication generates heat so inlets for cooling are located on the side of the cup. The sound enclosure is highly recommended for all cup horn users. In addition, to reducing sonication noise to safe levels, it securely supports the cup horn in the proper position. The sound enclosure features ports on either side to allow coolant tubing to pass from the cup horn to a water source or pump system outside the box.

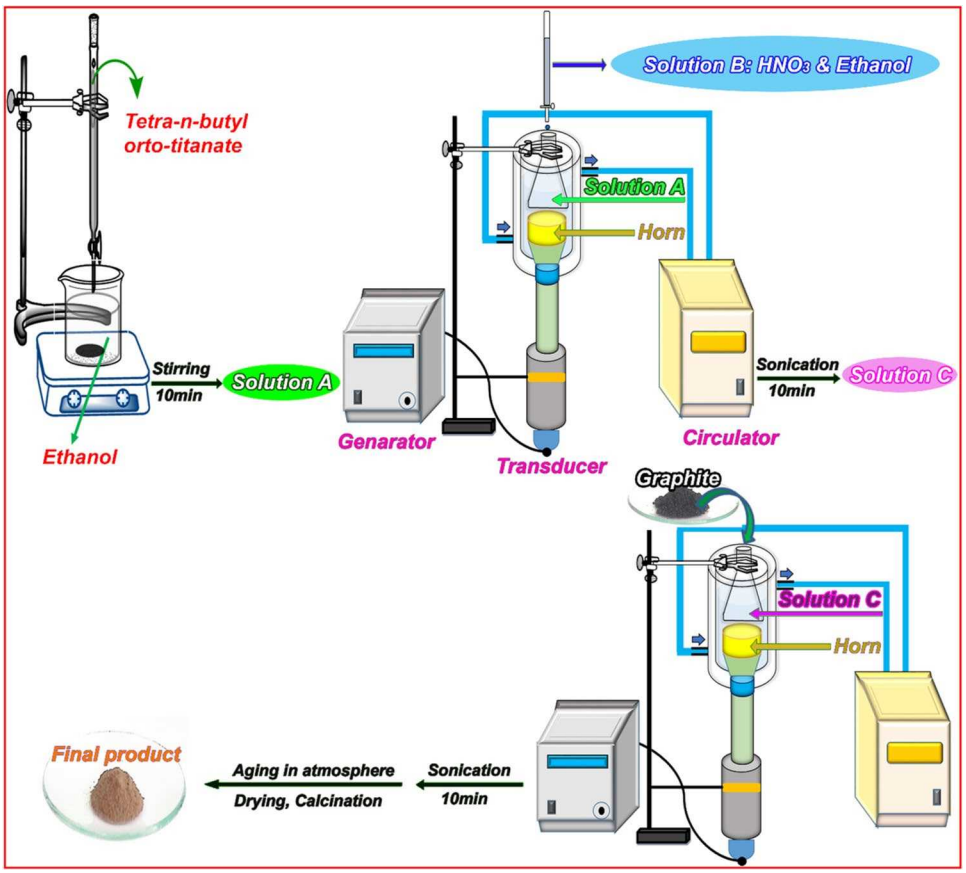

Fig. 1 Synthesis process of G/C-doped TiO_2 composite

Isoelectric point

The drift method was used to determine the pH of the isoelectric point of the synthesized nanocomposite. First, eight samples were prepared by adding 0.05 g of the nanocomposite in 30 mL of deionized water separately. After mixing for 5 min, their pH was adjusted with 0.01 M HCl solution for the acidic and with 0.01 M NaOH solution for the basic mixtures. The prepared mixtures were kept at 25 °C for 48 h and then their pH was measured again and the ΔpH was plotted versus the initial pH.

Characterization methods

The obtained materials were identified using several techniques. The crystalline phase of the samples was identified by X-ray diffraction (XRD-D8 Advance, Bruker-axis, pattern of materials was assembled in the area of 20°–80° in a scanning rate of 0.04°/s, armed with Cu Kα radiation, $\lambda = 1.5406$ Å). The Fourier transform-infrared (FTIR) spectra were obtained with KBr disks including the powder sample by the FTIR spectrometer Thermo Nicolet (Avatar 370). Diffuse reflectance spectrum (DRS) was carried out by the Scinco 4100 apparatus to determine the photochemical characteristics of the synthesized materials. The photoluminescence (PL) spectroscopy was performed with a PerkinElmer ls45. The X-ray photoelectron spectrum (XPS) was recorded to investigate the binding energy and chemical composition of the sample with the German BES-TEC model instrument using monochromatic Mg Kα irradiation (1253.6 eV) to get knowledge of the composition, chemical bonds, and relative proportions of the different elements. UV–vis spectra of all samples were done by using a UV–Vis spectrophotometer, Unico 2800. The morphology and particle size of the sample were determined via scanning electron microscopy (SEM) and transmission electron microscopy (TEM) measurements using a Leo 912 AB, Germany, voltage 120 kW which was equipped with an X-ray energy-dispersive spectroscopy (EDS). High-resolution microscopy (HRTEM) (FEI Tecnai G2 F20 Super Twin TEM (acceleration voltage: 200 kV)) and the selected area electron diffraction pattern (SAED) of the sample were used to investigate the microstructure and revealed the presence of phase in the sample. The Brunauer–Emmett–Teller (BET) surface areas of samples were measured with a Toosnano Gassorb 1 apparatus (Micromeritics, IRAN) in a relative pressure range from 0.0 to 1.0. Nitrogen adsorption–desorption isotherms were performed by a Micromeritics Toosnano Gassorb 1 instrument at 77.30 K. Total organic carbon (TOC) was measured with a Shimadzu VCPH/CPN analyzer.

Photocatalytic experiments

To investigate the performance of the photocatalytic activity of different samples, DCF was selected as a model pollutant. Photocatalytic experiments were performed for all synthesized materials at room temperature in a cylindrical Pyrex reactor with about 100 mL capacity. Firstly, 0.05 g of the prepared catalyst was added to 30 mL of 10 mg L^{-1} DCF solution. According to the conducted research, among different groups of medicine painkillers, DCF has the lowest concentration in sewage, effluent, and water samples. According to the research conducted in Iran, the amount of DCF in real water is 0.034 μg L^{-1}. By comparing with the concentration value that we investigated in the laboratory, the synthesized sample can easily and quickly destroy low amounts of theses of 10 mg L^{-1} (Khetan and Collins 2007; Mortazavi and Norouzi Fard 2017). The solution was magnetically stirred in the dark for 90 min to attain adsorption/desorption equilibrium between DCF and nanophotocatalyst. A 1.31×10^{21} photons/s short-arc xenon lamp was used as a visible light source. It was installed inside the box at a distance of about 5 cm next to the reaction system (photoreactor). Next, the prepared reaction sample was exposed to xenon light and sampling was done at different times (10, 20, 30, and 50 min). The removed samples were centrifuged for 5 min at a speed of 10,000 rpm and the absorbance of the upper solution was recorded at 276 nm by a UV–Vis spectrophotometer. To investigate the role of each active species in DFC degradation, similar samples with 10 mg L^{-1} of DCF were prepared, and 0.05 g of catalyst was added to each sample. Next, a certain concentration (10 mmol L^{-1}) of the scavengers (para-benzoquinone (BQ), methanol, and tetra-butyl alcohol (TBA) as the scavengers for trapping the active species $^{\bullet}O_2^-$, h^+, and $^{\bullet}OH$, respectively) were added to each of the samples and the samples were exposed to xenon light for 50 min; the absorption of the samples was obtained and the main active species in DFC degradation was determined.

Results and discussion

Characterization of optimized G/C-doped TiO_2

XRD analysis

XRD technique is a very fast and analytical method used to identify the phase of crystalline material and chemical compounds. The diffraction patterns related to the G and G/C-doped TiO_2 in the scale of $2\theta = 20°–80°$ are shown in Fig. 2(a, b). Diffraction peaks at 26.5°, 43.3°, 44.5°, 54.6°, and 77.4° are related to (002), (100), (101), (004), and (110) G plates, respectively (Panjiar et al. 2015), which correspond to the standard card of 41–1487 from the Joint Committee on Powder Diffraction Standards (JCPDS). G/C-doped TiO_2 and TiO_2 diffraction peaks at $2\theta = 25.5°$, 37.8°, 47.9°, 54.4°, 62.7°, 68.9°, and 75° related to the anatase phase, peak diffraction at $2\theta = 30.9°$ confirms the formation of brookite phase (Chen et al. 2013; Jia et al. 2016), and diffraction peaks at $2\theta = 36.2°$ and 42.3° are attributed to the formation of rutile phase (Ojeda et al. 2017). The appearance of a diffraction peak at about $2\theta = 26.5°$ in the sample synthesized by the ultrasonic waves corresponds to the G plate (002) (Yu et al. 2014). Meanwhile, the effective grain size of the as-prepared samples was calculated by the Debye–Scherrer formula on the anatase (101) diffraction peaks (Chen et al. 2013).

$$D = \frac{K\lambda}{\beta \cos\theta} \quad (1)$$

where K (0.94) is a shape factor, λ the wavelength of Cu Kα radiation ($\lambda = 0.15418$ nm), β the full-width at half-maximum (FWHM) of the main intensity peak, and the θ angle of diffraction. The average crystallite size of the TiO_2 sample was found to be 8.7 nm.

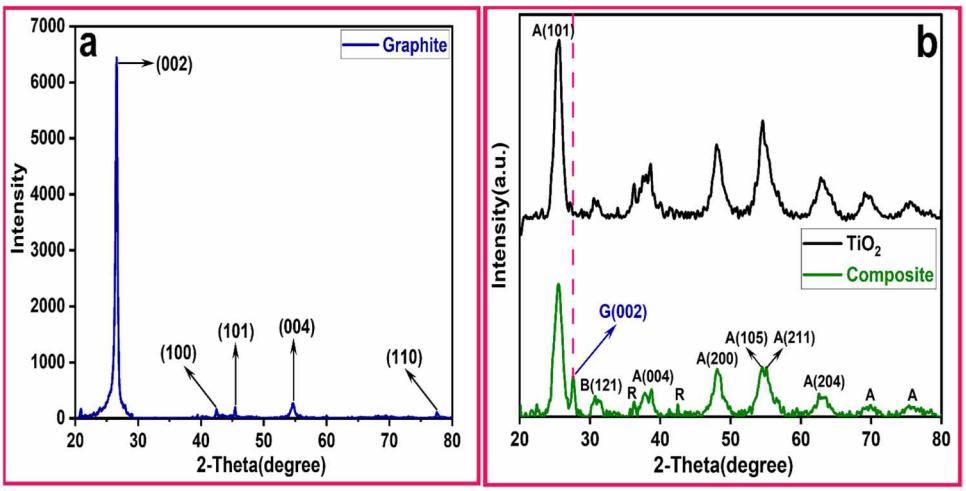

Fig. 2 XRD patterns of G (**a**) and G (0.03 g)/C-doped TiO_2 nanocomposite, and TiO_2 (**b**)

FTIR analysis

FTIR spectra of the G, TiO_2, and G/C-doped TiO_2 composite were conducted and shown in Fig. 3. In G, the bands at 1043 cm^{-1}, 1594 cm^{-1}, and 3670 cm^{-1} were related to C–O, C = C, and –OH stretching vibrations, respectively (Chen et al. 2013). In two samples of TiO_2 and synthesized composite, the peak at about 690 cm^{-1} is related to the stretching vibration of Ti–O and Ti–O–Ti bonds (Shen et al. 2011a). The broad peak appearing at the wavenumber of 3400 cm^{-1} and the small peak at 1600 cm^{-1} correspond to the stretching vibration of the hydroxyl group (O–H) related to water (Li et al. 2005). The specific peaks of the G and TiO_2 were still existing in the G/C-doped TiO_2 composite. The strong and broad peaks in the range of 500–1000 cm^{-1} are attributed to the as-prepared TiO_2 and the synthesized nanocomposite. The Ti–O–C low-frequency band peak in the composite around ~ 798 cm^{-1} overlaps with the stretching vibrational states of Ti–O–Ti (Djellabi et al. 2019b, a). The presence of Ti–O–C bonds confirms that chemical bonds have formed between graphite and TiO_2 nanostructures in the composite (McDevitt and Baun 1964). Therefore, it is assumed that graphite can be well combined with TiO_2 by using ultrasonic waves, which is in agreement with the data achieved from XRD.

SEM analysis

Morphological profiles of graphite (G) and G (0.03 g) /C-doped TiO_2 composite were investigated by SEM. SEM images of G and G/C-doped TiO_2 composite are shown in Fig. 4a and 4b, respectively. As shown in Fig. 4a, the G was looking like pieces of paper to some degree and seemingly several few layers which were overlapped and had irregular morphology with a smooth surface. Figure 4b shows that TiO_2 was composed of aggregates of primary particles of different sizes. Therefore, after a combination of G with TiO_2, its surface is very smooth, indicating that the TiO_2 sol precursor fills all the pores of the G when the first layers are deposited and then forms a uniform thin film on the top of G (Jia et al. 2016). The EDS study (Fig. 4c) distinctly indicates that the photocatalyst is a compound of Ti, O, as well and C. It is noteworthy that C–O groups were formed on the surface graphite due to slight oxidation of graphite. Hence, the atomic percent of the O element can be attributed to the Ti–O and C–O bondings.

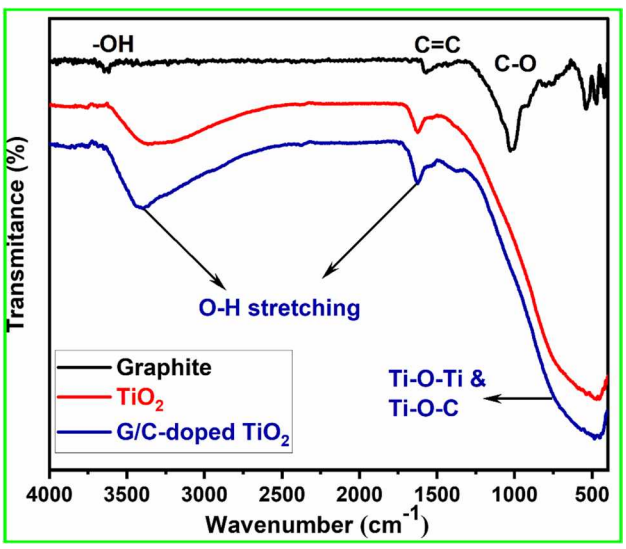

Fig. 3 FT-IR spectrum of G, TiO_2, and G (0.03 g)/C-doped TiO_2 nanocomposite

TEM and HRTEM analysis

TEM images of G/C-doped TiO_2 nanocomposite are shown in Fig. 5a and b. As can be seen in Fig. 5a, multilayered graphite plates were completely covered with C-doped TiO_2 nanoparticles with uniform size distribution. The TEM image in Fig. 5b clearly shows the graphite layer and spherical C-doped TiO_2 nanoparticles. Under sonication, C-doped TiO_2 nanoparticles with homogneous size distribution formed on the graphitic sheets (Mason 2003; Colmenares et al. 2006). The size of the TiO_2 nanoparticles was about 10 nm, which is in agreement with the X-ray pattern and SEM images. Figure 5c shows the HRTEM profile of the G/C-doped TiO_2 nanocomposite. HRTEM analysis indicates two d-spacings of 0.34 nm and 0.33 nm, which are assigned to the planes (101) and (002) of TiO_2 and graphite, respectively (Zhang et al. 2008; Wang et al. 2010; Inagaki 2012).

According to the SEAD pattern of the G/C-doped TiO_2 nanocomposite displayed in Fig. 5d, the resulting nanocomposite has a polycrystalline nature. Diffraction rings of the planes (101) and (002) were observed in the SEAD pattern, which refers to the tetragonal structure of TiO_2 anatase and graphite, respectively.

XPS analysis

To study the surface composition and chemical states of the conceivable dopants incorporated into TiO_2, the binding energies of Ti_{2p}, O_{1s}, and C_{1s} are illustrated in XPS (Fig. 6). Figure 6a shows the comparative full-scale XPS survey spectrum of the as-prepared G/C-doped TiO_2 composite. Specifically, the sample contained Ti, O, and C elements with sharp binding energies at about 464.47 eV (Ti_{2p}), 534.76 eV (O_{1s}), and 289.52 eV (C_{1s}), respectively. Figure 6b shows the deconvolution of the Ti_{2p} spectrum with two symmetrical peaks appearing at binding energies of 469.0 eV and 463.64 eV concerning $Ti_{2p1/2}$ and $Ti_{2p3/2}$, respectively, which ascribed to O–Ti–O bond in TiO_2. In this case, the binding

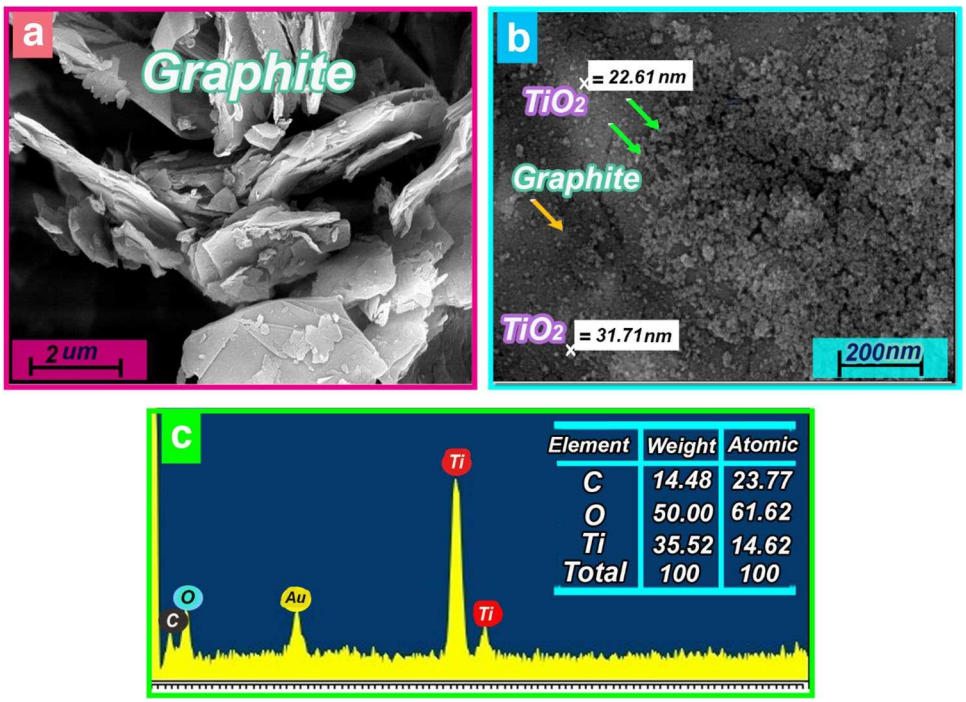

Fig. 4 SEM pictures of G (**a**), G/C-doped TiO_2 nanocomposite (**b**), and EDS spectrum of G (0.03 g)/C-doped TiO_2 nanocomposite (**c**)

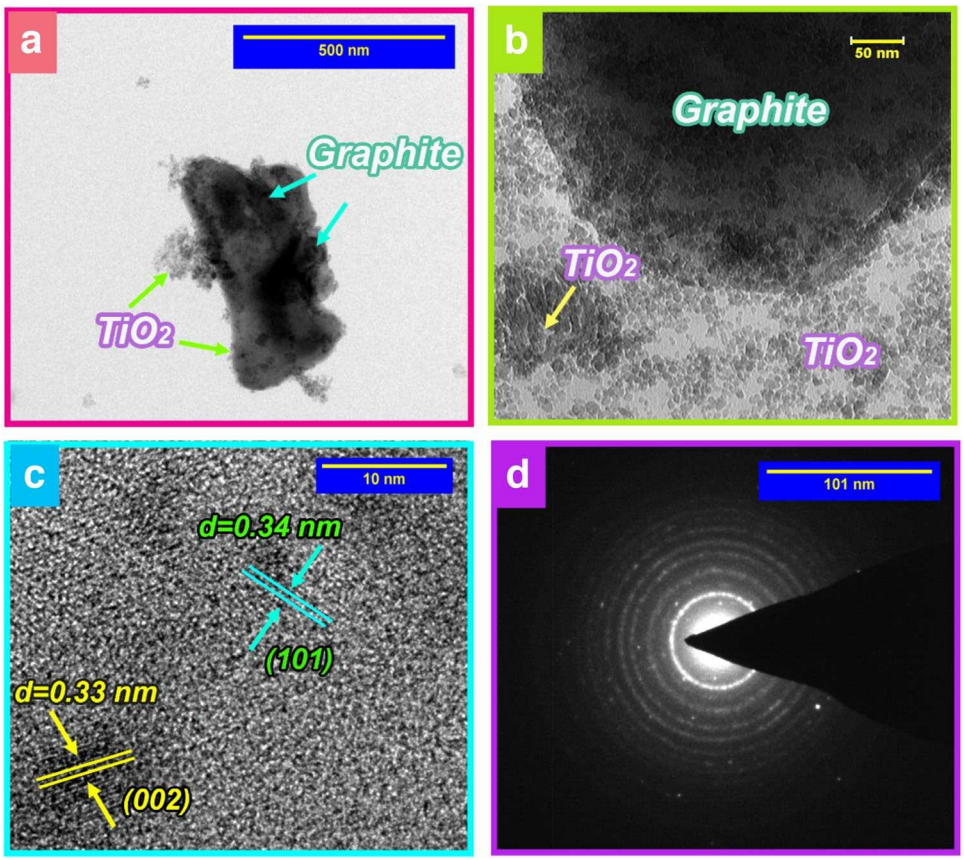

Fig. 5 **a**, **b** TEM images, **c** HRTEM profile, and **d** SEAD pattern of G (0.03 g)/C-doped TiO_2 nanocomposite

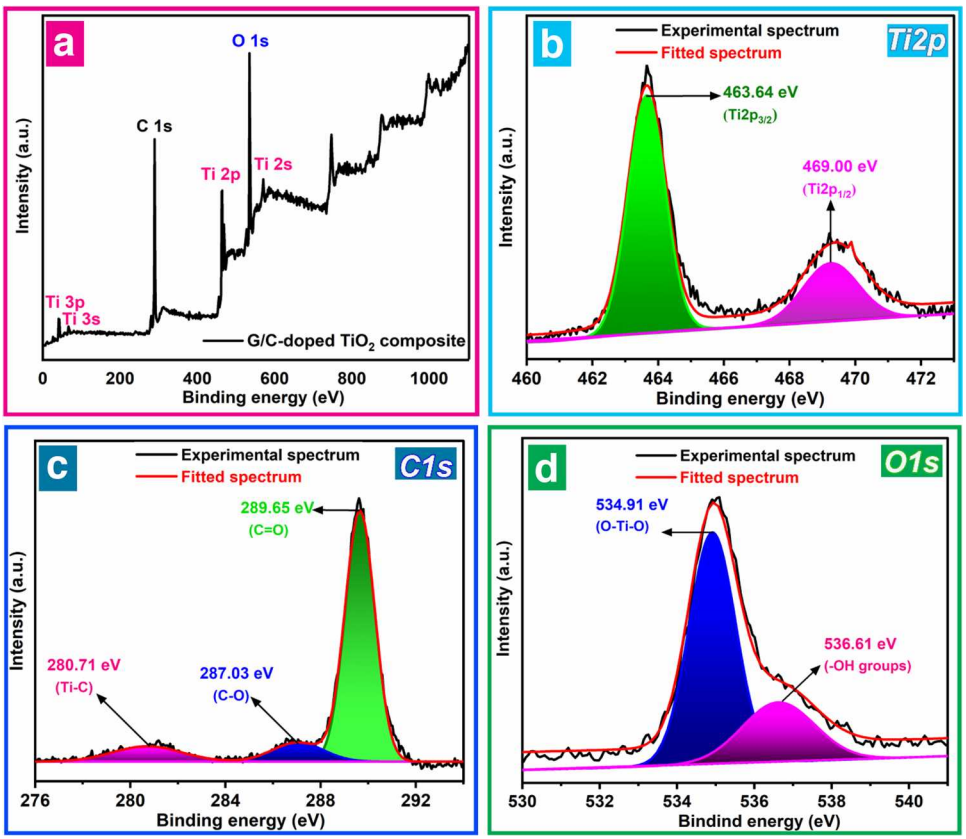

Fig. 6 Survey XPS (**a**), deconvolution of Ti_{2p} (**b**), C_{1s} (**c**), and O_{1s} (**d**) of the G (0.03 g)/C-doped TiO_2 nanocomposite

energy increases upon C-doping, strongly indicating lattice distortions (Mali et al. 2012; Zhang et al. 2015a; Dong et al. 2018). The difference of 5.36 eV between the two peaks might be assigned to the oxidation level of + 4 for the Ti element. Results are in agreement with other works (Neville et al. 2012). The deconvolution of XPS spectra of C_{1s} was performed to identify the chemical composition of C_{1s} in G/C-doped TiO_2 nanocomposite. Significantly, the C_{1s} binding energy peaks from the G/C-doped TiO_2 were widespread and asymmetric. This indicates the coexistence of the various chemical conditions of the C atoms due to their binding energies from 276 to 296 eV as observed in Fig. 6c. The basic band can be deconvoluted into three individual peaks concentrated around 280.71, 287.03, and 289.65 eV. The deconvoluted C1s peak in binding energy of 280.71 eV can be assigned to the O–Ti–C bonds. This displays that C was doped in the TiO_2 lattice by replacing some of the lattice oxygen atoms (Yang et al. 2009; In et al. 2009; Yu et al. 2011, 2013; Etacheri et al. 2013; Zhang et al. 2015a; Li et al. 2020b). Based on the theoretical prediction of Di Valentin et al. (2005), the introduction of the C atom into the TiO_2 lattice leads to localized states in the middle of the TiO_2 bandgap. Such states should extend the visible light absorption of the doped TiO_2. The two other C1s peaks that emerged at 287.03 and 289.65 eV were related to the oxygen-bound species such as C–O and C = O, respectively (Amalraj Appavoo et al. 2014; Li et al. 2015b). Therefore, different carbon species such as substitutional and interstitial carbon atoms and carbonate species exist in the TiO_2 lattice (Kim 1990; Amalraj Appavoo et al. 2014; Li et al. 2015b). These results confirm that graphite effectively interacted with TiO_2 nanoparticles and it was consistent with the various analyses such as XRD, SEM, TEM, and HRTEM. The deconvolution of the O_{1s} spectrum of nanocomposite is demonstrated in Fig. 6d. The spectrum is wide and asymmetric and it could be decomposed into two peaks. The first peak at 534.91 eV is ascribed to the O–Ti–O bond in the TiO_2 framework, whereas the second peak around ~ 536.61 eV is attributed to the hydroxyl groups (–OH) resulting mostly from chemisorbed H_2O (Zhu et al. 2017; Liu and Li 2018).

DRS analysis

The absorption properties of graphite (G), TiO_2, and G (0.03 g) /C-doped TiO_2 nanocomposite were analyzed and illustrated in Fig. 7. Figure 7(a) indicates the UV/vis DRS of the synthesized samples. Carbon-based materials usually show a broad peak (π-π^*) that appears in the range of 200–300 cm^{-1} (UV region) and it is attributed to sp^2 hybridization (C = C bond). The location of this peak shifts to the visible area by increasing the sp^2 characteristic through its combination with other materials (Shen et al.

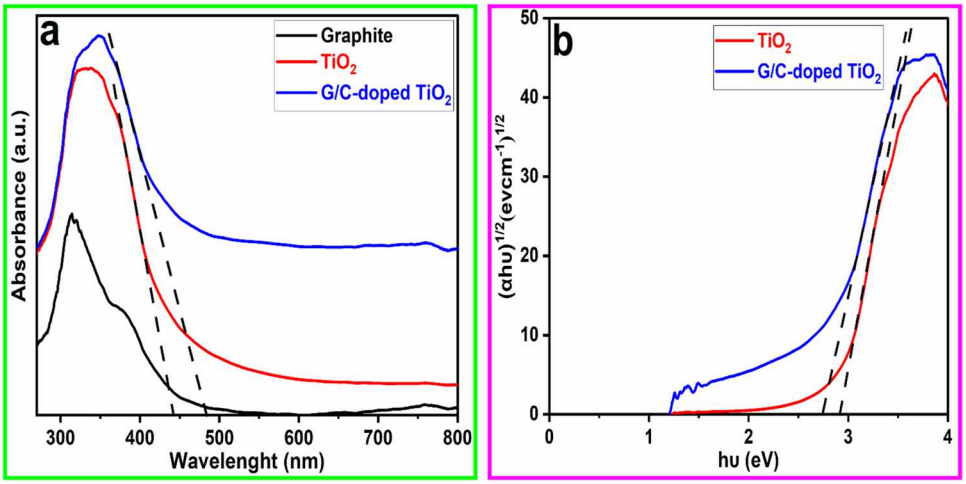

Fig. 7 **a** UV/vis diffuse reflectance spectrum, **b** plots of $(\alpha h\nu)^{0.5}$ against photo energy of the fabricated G, TiO_2, and G (0.03 g)/C-doped TiO_2 nanocomposite

2011b; Güler et al. 2016). Pure TiO_2 exhibited little visible light absorption. In comparison with the pure TiO_2, the improved absorption in the whole visible light region of the G (0.03 g)/C-doped TiO_2 composite is related to the electron transport from the O^{-2} antibonding orbital to the lowest unoccupied Ti^{+4} orbital ($O_{2p} \rightarrow Ti_{3d}$) (Li et al. 2015a). An intense absorption of samples with a wavelength less than 380 nm can be ascribed to the absorption of the inherent band gap of TiO_2 due to electronic transmission from the valence band (VB) to the conduction band (CB). TiO_2 and G/C-doped TiO_2 nanocomposite show wide light absorption in the 380 to 800 nm range, which was similar to the previous reports of TiO_2 nanotubes (Zhuang et al. 2007; Xu and Yu 2011). TiO_2 absorbs slightly the visible light and the absorption enhancement of TiO_2 nanocomposite across the visible light region can be related to the incorporation of G in TiO_2. Furthermore, the formation of the nanocomposite caused a bit shift in the visible light region due to the creation of C–O or C = O bonds and the hybridization of the atomic orbitals of C_{2p} and O_{2p} between the G and TiO_2 interface (Zhang et al. 2014b; Ojeda et al. 2017). The absorption spectra are displayed in Fig. 7(a). The tangent drawn demonstrates the maximum absorption at 447 nm and 487 nm for the TiO_2 and G/C-doped TiO_2 nanocomposite that matched the band gap of 2.97 eV and 2.75 eV, respectively. The edge energy for the as-prepared materials was obtained through the application of Tauc's law. In 1966, Tauc and his team proposed the law into a simple relationship that is now known as Tauc's law. The so-called Tauc's method can be used to estimate the Eg of semiconductors from the optical absorption spectra obtained by UV–vis spectroscopy, and can apply to amorphous and crystalline nanomaterials. The band-gap energy was estimated by plotting $(\alpha h\upsilon)^{1/n}$ as a function of the photon energy ($h\upsilon$), where h is the Planck constant, ν is photon's frequency, Eg is bandgap energy, C is a constant, and α is the absorption coefficient which describes how much light of a given color is absorbed by a material of given thickness. The n is a factor that depends on the nature of the electron transition and is numerically equal to 1/2, 3/2, 2, or 3 for direct allowed, direct forbidden, indirect allowed, or indirect forbidden transitions, respectively (Tauc et al. 1966; Coulter and Birnie 2018). The results are illustrated in Fig. 7(b). Therefore, based on the obtained results, it can be concluded that combining TiO_2 and graphite and modifying the performance of TiO_2 to perform photocatalytic reactions in the visible region will be very desirable.

PL spectroscopy

The recombination of free carriers (positive holes and the photoinduced electrons) after irradiating the sample by visible light or UV causes the emission of photons that generate the characteristic PL peaks (Thomas et al. 2014). As shown in Fig. 8, the TiO_2 emission spectra have a higher relative intensity than nanocomposite and it means that electrons and holes again recombine more easily in TiO_2 than nanocomposite. The combination of TiO_2 with G and the formation of nanocomposite significantly reduce the intensity of the PL. This decrease in spectral intensity in the nanocomposite relative to TiO_2 has been attributed to the G that can transfer photoinduced electrons rapidly and prevent hole/electron recombination which is important in increasing photocatalytic degradation (Huang et al. 2013a, 2014; Gao et al. 2014). In addition, the photocatalytic activity of nanocomposites increases with increasing the amount of G to the optimum value (0.03 g) and then decreases.

BET analysis

The BET specific surface area and porous structure characteristics of various samples were determined using nitrogen isothermal adsorption. Figure 9a–e shows nitrogen adsorption/desorption isotherms of the TiO_2 nanoparticles, G-0.01 g, G-0.03 g, G-0.05 g, and G-0.10 g, respectively.

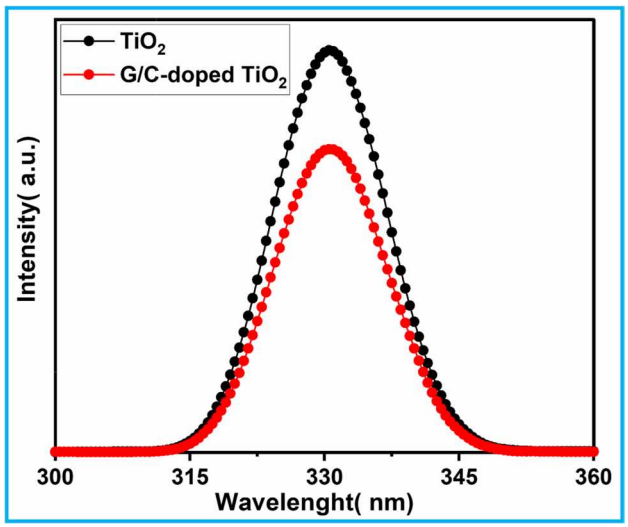

Fig. 8 Photoluminescence spectra of TiO_2 and G (0.03 g)/C-doped TiO_2 nanocomposite

All the photocatalysts exhibit the type IV physisorption isotherm and H_2 hysteresis loop indicating a mesoporous material (Zhu et al. 2021). Their corresponding specific surface areas are 329, 342, 443, 422, and 359 m^2/g for TiO_2, G-0.01 g, G-0.03 g, G-0.05 g, and G-0.10 g, respectively. The surface areas were increased significantly with the addition of graphite compared with TiO_2. It is believed that the large specific surface area facilitates better access and diffusion of liquid and gaseous reactants which is beneficial for photocatalytic reactivity. The specific surface area results reveal that the G-0.03 g sample shows a higher surface area than pure TiO_2. Sibu et al. (2002) and Adyani and Ghorbani (2018) claim that the surface textural property is improved owing to the presence of Ti–O–M (M is the doping element) bonds, which may restrain the conformity and rearrangement of primary crystals, leading to increase of surface area (Li et al. 2016b; Makal and Das 2018). The BET level was lower in the case of the G-0.10 g sample due to the higher particle agglomeration. These results revealed that the addition of graphite was significantly effective for increasing a specific surface area of the photocatalyst, which was higher than that of pure TiO_2. This characteristic causes more effective contact surfaces between the photocatalyst and reactant. The higher surface area has the better photocatalytic activity.

The isoelectric point of the nanocomposite

The prepared mixtures were kept at 25 °C for 48 h and then their pH was measured again and the ΔpH was plotted versus the initial pH (Fig. 10a). The pH of the isoelectric point of the synthesized nanocomposite was 6.59, which at this point, the initial value of pH is equal to its final value (Prahas et al. 2008).

Considering that in a mixture, the surface charge and the absorption of organic substances depend on its pH. Hence, the photocatalytic degradation of DFC as an organic matter also depends on the pH of the mixture. In an experiment called pH effect, the photocatalytic degradation of DFC was investigated in an aqueous suspension in the pH range of 1.5 to 10. Figure 10b shows the decomposition of DCF at different pH. Reactions (2) and (3) show the protonation and deprotonation of the TiO_2 semiconductor surface in the acidic and basic media, respectively (Qamar and Muneer 2009).

$$TiOH + H^+ \rightarrow TiOH_2^+ \tag{2}$$

$$TiOH + OH^- \rightarrow TiO^- + H_2O \tag{3}$$

According to the obtained results, the pH of the isoelectric point for G/C-doped TiO_2 nanoparticles was equal to 6.59. Therefore, the photocatalyst surface is positive at a pH lower than this value and negative at a pH higher than this value. A better performance and efficiency for DCF degradation occur under light at its natural pH (6.75). One of the features and characteristics of DCF is that it has a pK_a of about 4, which is attributed to its carboxylic group (Lara-Pérez et al. 2020; Zaka et al. 2021). Therefore, under very acidic conditions, DCF charges positively which is similar to the surface charge of the photocatalyst, and an electrostatic repulsive force develops between them. Also, as in acidic conditions, the electrostatic repulsive force is created in basic conditions due to a similar charging of the photocatalyst surface and DCF. Hence, The electrostatic forces between the negatively charged carboxylate group of the DCF molecule and the positive charge of the solid surface favor the interaction between both chemical species (Bhadra et al. 2016a, b; Lara-Pérez et al. 2020). It can be concluded that at normal pH, due to the interaction between the photocatalyst and DCF, the photocatalyst surface charge becomes positive by the carboxyl group of the DCF loses a proton and causes the negative charge on the DCF. The G/ C-doped TiO_2 composite surface has a positive charge and one of the oxygen atoms of the carbonyl group of the DCF molecule is negatively charged. Therefore, experimental conditions favor the electrostatic interaction between G/C-doped TiO_2 composite catalysts and the organic molecule as previously reported (Zhang et al. 2014a; Boukhatem et al. 2017). By performing this action, attractive forces are formed and cause the effective absorption of DCF pollutants on the photocatalyst surface. This leads to improving the degradation efficiency of the target pollutant.

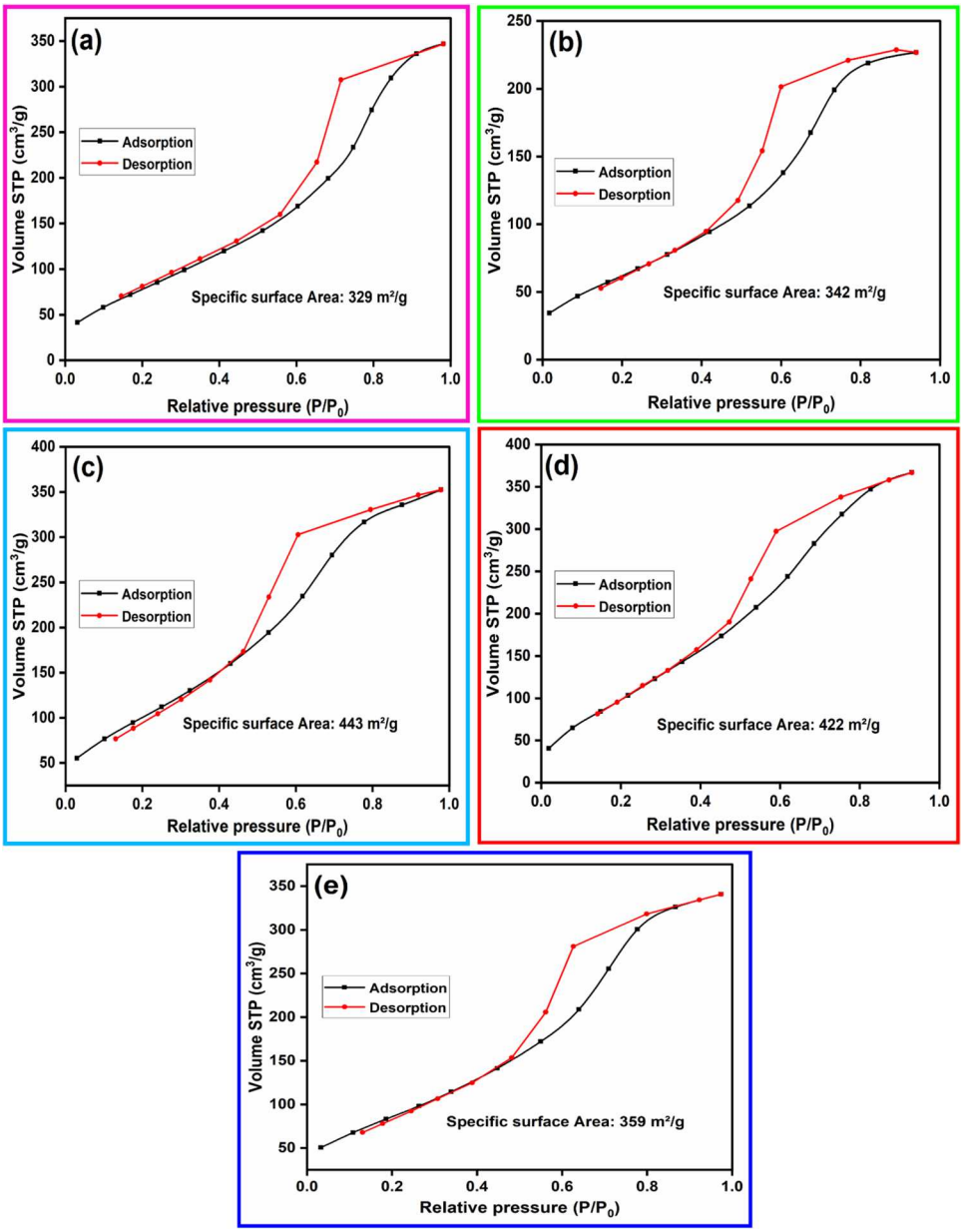

Fig. 9 Nitrogen adsorption–desorption isotherms of a pure TiO_2 (**a**), G–0.01 g (**b**), G–0.03 g (**c**), G–0.05 g (**d**), and G–0.10 g (**e**)

Photocatalytic performances

The photocatalytic activity of the as-prepared nanocomposite was evaluated in the decomposition of DCF contaminant under three conditions darkness, photolysis, and the simultaneous presence of catalyst and xenon light. Figure 11a and b indicate the scans of UV–vis spectra of 10 mg L^{-1} DCF in darkness (in the presence of catalyst) and light (without catalyst), respectively. As displayed in Fig. 11a, the intensity of the absorption peak at 276 nm gradually decreases and then stabilizes as the time in the dark increases to 90 min. Therefore, the optimal dark time for different samples was 90 min. As shown in Fig. 11b, after a relatively long time (160 min), the amount of pollutant degradation in the presence of light is very low. Therefore, it is concluded that light alone does not have impressive efficiency in the decay of the DCF contaminant. Figure 11c shows a sharp decrease in the intensity of the absorbance peak of DCF with increasing the reaction time. It takes 50 min for the complete degradation of DCF in the solution at pH 6.75 while about 60% of total organic carbon (TOC) was removed under the same conditions. For the comparison, the photocatalytic performance of the sample synthesized by the sol–gel method was compared with the sample prepared under ultrasound in the degradation of DCF under the same conditions. The degradation was completed in about 420 min for the sample prepared in the sol–gel method.

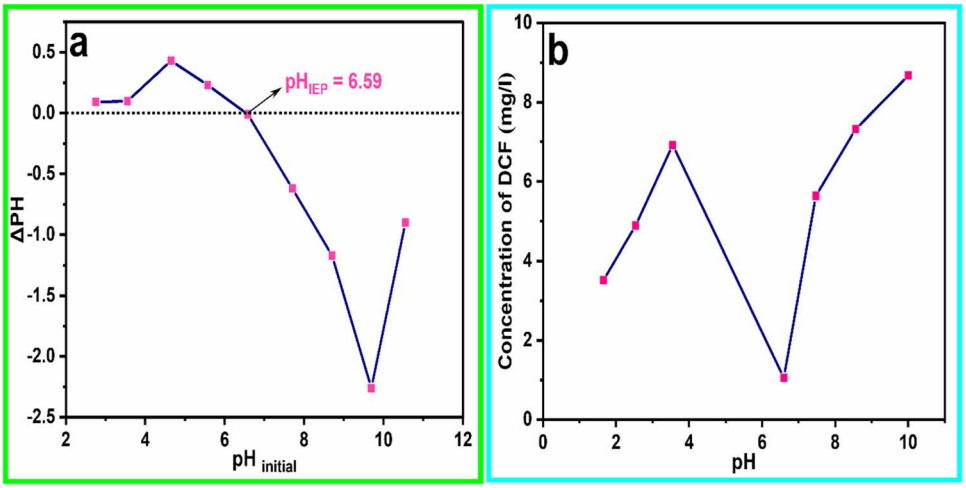

Fig. 10 **a** pH_{IEP} determination using pH Drift method and **b** pH effects on the decomposition of DCF by G (0.03 g)/C-doped TiO_2 composite (initial concentration: 10 mg L^{-1}, temperature: 25 °C, amount of catalyst: 0.05 g, irradiation time: 50 min)

Therefore, the use of ultrasound in the synthesis improved the photocatalytic performance of the sample. A peak displacement that occurs in the G/C-TiO_2 nanocomposite/light system during DCF degradation was related to the formation of intermediate species (Di Credico et al. 2015). Numerous studies have shown that intermediate molecules are produced during the degradation of DCF in the presence of light (García-Araya et al. 2010; Keen et al. 2013; Michael et al. 2014; Boukhatem et al. 2017; Schulze-Hennings et al. 2017). Intermediates were identified by Moctezuma et al. (2020). Several intermediates were identified, essentially fumaric acid, 2-aminophenol C11, pyrocatechol C14, pyrogallol C13, and 2,6-dichloroaniline C4. Fortunately, in this study after 50 min there are no peaks for the intermediates. The spectra in the presence of nanocatalysts are approximately the same. The intermediates are not stable and after 50 min (Fig. 11c); there is no peak in the UV spectrum. Also, the concentration of intermediates may be so low that it does not show itself. The high degradation efficiency and complete decomposition are greatly attributed to the synergistic effects of combining graphite with TiO_2 carbon doping in the nanocomposite. Figure 11d shows the UV–vis spectra of DCF in an aqueous solution in the presence of TiO_2 NPs at different interval times. As this figure shows the complete photodegradation of the DCF by pure TiO_2 NPs took place within 140 min. G-0.03 g shows higher photocatalytic efficiency than pure TiO_2 because of its lower recombination rate and higher surface area compared to pure TiO_2 NPs. Therefore, compositing graphite with TiO_2 nanostructures effectively promotes visible light absorption which can be attributed to electronic interactions or chemical bonding between G and TiO_2 nanostructures. Figure 11e shows that 100% of DCF was degraded by G (0.03 g)/C-doped TiO_2 within 50 min, whereas the complete degradation of DCF occurred within 140 min and 120 min for pure TiO_2 NPs and P25 TiO_2, respectively. The degradation of DCF can be described by a pseudo-first-order reaction expression with a simplified Langmuir–Hinshelwood model (Eq. 4). The k_{app} for photocatalytic degradation of DCF was calculated to be 0.06061 min^{-1}, 0.03924 min^{-1}, and 0.02926 min^{-1} for G (0.03 g)/C-doped TiO_2, P25 TiO_2, and pure TiO_2, respectively, which the photocatalytic degradation efficiency of DCF follows G (0.03 g)/C-doped TiO_2 > P25 TiO_2 > pure TiO_2.

G/TiO_2 ratio on the degradation

Figure 12 displays the degradation of DCF versus time under xenon light using various synthesized nanocatalysts. The degradation of DCF was 8.57% in photolysis; 95.26%, 96.45%, 95.02%, 95.79%, and 95.42% by nanocomposite containing G-0.01 g, G-0.03 g, G-0.05 g, G-0.10 g, and TiO_2 nanoparticles within 160-, 120-, 50-, 160-, 200-, and 140-min xenon light irradiation, respectively. First, the decomposition of DCF was investigated under light without the presence of the catalyst (photolysis) and the amount of decomposition was negligible. Secondly, the absorption of DCF was measured in the optimum dark time (90 min) as a control for different G/TiO_2 ratio nanocomposites, and absorption was obtained at 3.4, 23.7, 5.7, and 6.9% by nanocomposite containing G-0.01 g, G-0.03 g, G-0.05 g, G-0.10 g, respectively. Then different samples were followed by xenon light irradiation. Based on Fig. 12a, the nanocatalyst synthesized with 0.03 g of G (G-0.03 g) shows the highest rate of DCF degradation in comparison with other samples having different ratios. The adsorption kinetics for the degradation of DCF was studied using the pseudo-first-order model. The rate constant for photodegradation was evaluated using the following equation:

$$-\ln\frac{C_t}{C_0} = k_{app}t \quad (4)$$

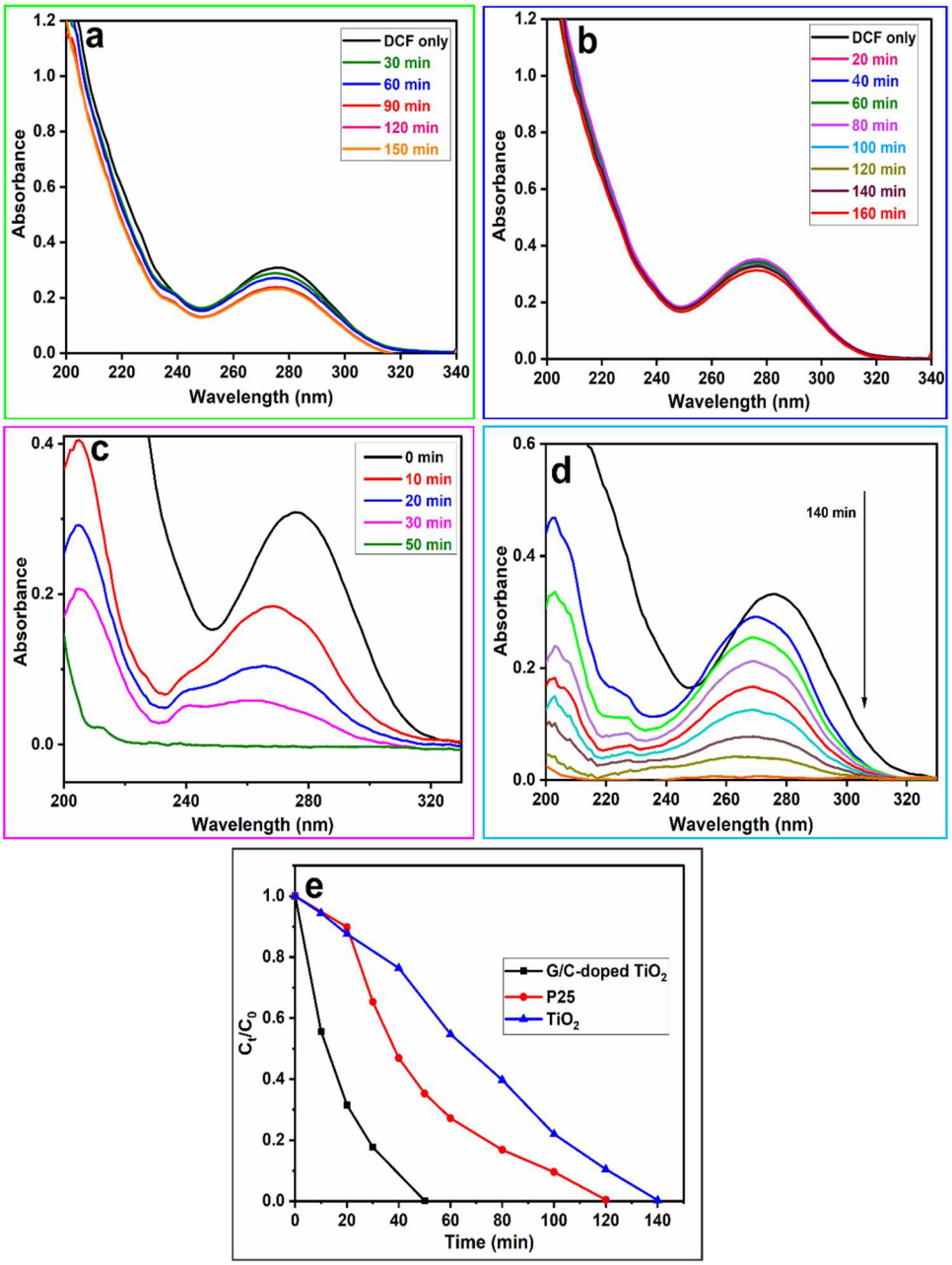

Fig. 11 UV–vis absorption spectra of DCF: **a** in the presence of catalyst and darkness, **b** photolysis (only light), **c**, **d** degradation of DCF as a function of the irradiation time by using the G (0.03 g)/C-doped TiO_2 as a photocatalyst and synthesized TiO_2, respectively. **e** The comparative studies for P25, TiO_2, and G (0.03 g)/C-doped TiO_2 ($C_o = 10$ ppm, pH: 6.75, the dose of catalyst = 0.05 g)

where C_0 and C_t are the initial concentration of the dye and concentration of the dye at time t, respectively, and k_{app} is the apparent rate constant for the pseudo-first-order photo-degradation reaction. Figure 12b shows the plot of $-\ln(C_t/C_0)$ versus time which represents a straight line and the slope of which is equal to the apparent first-order rate constant k_{app}. The effect of the initial concentration of the DCF monitored at 10 mg/L for a catalyst loading of 0.05 g is represented in Fig. 12b. The decrease in photo-catalytic activity can be attributed to the interference in light absorption with an increasing molar ratio of G/TiO_2. By increasing the amount of graphite, light absorption by the TiO_2 semiconductor to produce charge carriers (electron–hole) decreases and the degradation rate decreases. The improvement of photocatalytic activity to the optimum value can be explained by the fact that modification with graphite could promote the transfer and separation of photo-generated charge carriers, enlarge visible light absorption, and increase crystallinity. Figure 12c shows the stableness and reusability of the best-synthesized sample in six cycles. As Fig. 12c shows, the graphite/C-doped TiO_2 sample not only has excellent photocatalytic activity in the degradation of DCF but also has very good stability in pollutant degradation. The photocatalytic activity of the nanocomposite in pollutant degradation

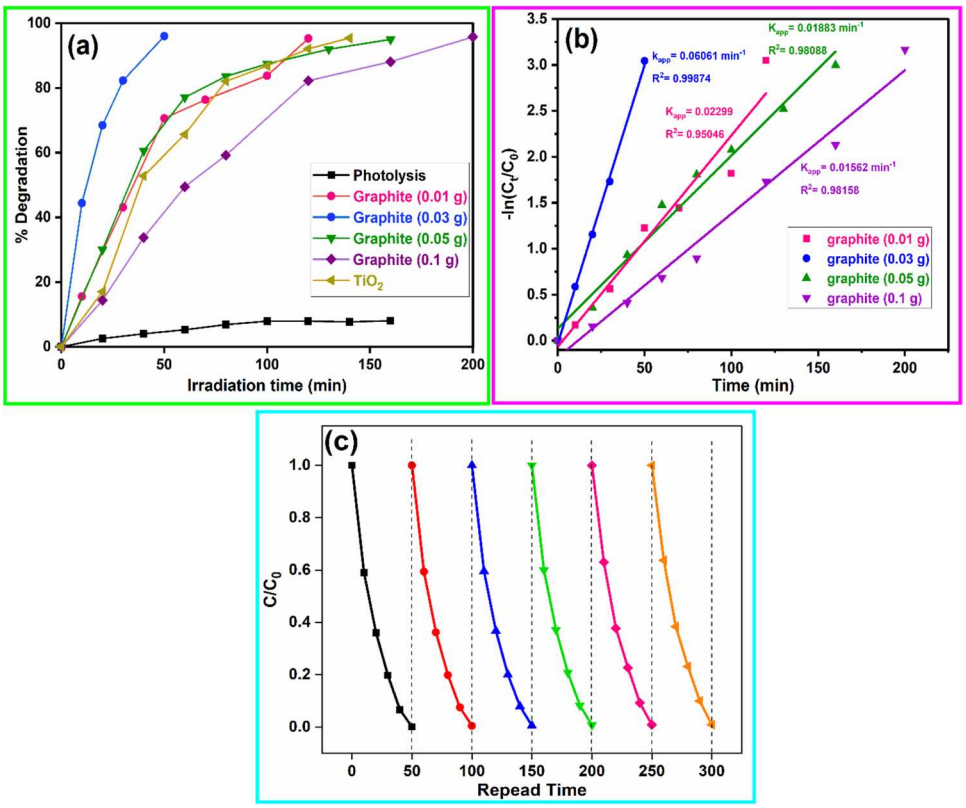

Fig. 12 **a** Photolysis and photocatalytic decay of DCF in the presence of differently prepared nanocatalysts (C_0, DFC: 10 mg L^{-1}, nanocatalyst: 0.05 g, pH: 6.75), **b** plot of pseudo-first-order kinetics model, and **c** recyclability test in different cycles using G (0.03 g)/C doped TiO_2 composite

decreases very little (about 4%) in six cycles, and this confirms that the synthesized sample can be used for long-term service without showing a clear decrease in pollutant degradation activity. This indicates that C-doping in TiO_2 improved the photocatalytic activity of TiO_2 under xenon light irradiation and thus promoted the degradation of DCF.

Comparative photocatalysis

To estimate the efficiency of the G/C-doped TiO_2 composite, its photocatalytic activity was compared with literature studies. As summarized in Table 1, compared with the reported other photocatalysts, the G/C-doped TiO_2

Table 1 Comparison with literature studies for photocatalytic degradation of DCF

Photocatalyst	Initial conc. (mg/L)	Removal (%)	Conditions	Ref
BiOCl–GO	25	47.88	Visible spectrum solar light. pH 5, time 180 min	Rashid et al. (2020)
O-gC_3N_4/TiO_2/α Fe_2O_3	10	100	Xe lamp. pH 6.75, time 60 min	Aghababaei et al. (2023a)
Ni–TiO_2	15	47	Solar UV lamp. time 120 min	Gil et al. (2017)
WO_3	0.5	100	Xe lamp. Time 120 min	Rey et al. (2015)
TiO_2–P25	2	100	Blacklight Philips TLK 05. time 60 min	Fabbri et al. (2019)
Ce–ZnO	2	100	Blacklight Phillips TLK 05. time 30 min	
TiO_2–SG	2	100	Blacklight Phillips TLK 05. time 30 min	
C_3N_4	10	19.3	Xe lamp. time 60 min	Liu et al. (2019)
CNC_2–C_3N_4	10	100	Xe lamp. time 60 min	
TiO_2–FeZ/H_2O_2	30	42.5	Xe lamp. time 180 min	Salaeh et al. (2016)
S-doping TiO_2	10	93	Visible light. time 240 min	Yi et al. (2019)
BiOCl–Au–CdS	20	100	Xe lamp. time 240 min	Li et al. (2017)
G/ C-doped TiO_2	10	100	Xe lamp, pH 6.75, time 50 min	This study

composite prepared in this work possessed excellent photocatalytic activity for DCF degradation. The shorter activity time of some catalysts may be attributed to the lower initial pollutant concentrations or the use of noble metal dopants (Li et al. 2017; Fabbri et al. 2019). Therefore, the results further demonstrated that the G/C-doped TiO_2 composite/light can be a promising system for organic pollutant degradation.

Effect of humic acid on DCF degradation

Degradation of DCF under xenon light irradiation in the presence of different concentrations of humic acid is shown in Fig. 13. It can be seen that the removal efficiency of DCF decreased when humic acid concentration increased. The complete DCF removal was accomplished within 50 min. When the humic acid concentration was 30, 40, 50, 60, and 80 mg/L, respectively, the removal efficiency of DCF was decreased. Humic acid is one of the commonly used natural organic matters (NOM), which could be decomposed by ionizing radiation and react with $^{\bullet}OH$ as following Eq. (5) (Arai et al. 1986).

$$^{\bullet}OH + RH_2 \rightarrow {}^{\bullet}RH + H_2O \quad (5)$$

Humic acid is a kind of complicated organic matter derived from humus. It is difficult to describe by a specific chemical formula, so we use RH_2 to represent humic acid. The $^{\bullet}OH$ radical could withdraw a hydrogen atom from an organic compound (RH_2) to produce $^{\bullet}RH$ radical, resulting in a chain reaction and the decomposition of humic acid. Humic acid as a hydroxyl radical ($^{\bullet}OH$) scavenger could compete with target organic pollutants for $^{\bullet}OH$ and inhibit the degradation of target pollutants.

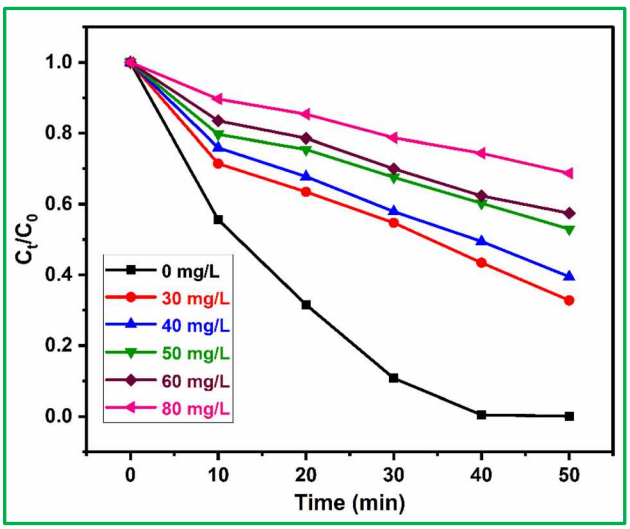

Fig. 13 Degradation of DCF at different humic acid concentrations (C_0, DCF: 10 mg L^{-1}, nanocatalyst: 0.05 g, pH: 6.75)

Photocatalytic mechanism

In a photocatalytic reaction, different species play a role in the degradation of a pollutant, which can be named $^{\bullet}OH$, $^{\bullet}O_2^-$, h^+, and H_2O_2 (Aghababaei et al. 2023b). To investigate the role of mentioned active species in the degradation of the desired pollutant, different active inhibitors (10 mmol L^{-1}) were applied for each active species separately (Li et al. 2016a). Figure 14 shows the degradation of DCF with a certain amount of the synthesized catalyst under normal conditions (without the presence of scavengers) and in the presence of different scavengers for each active species in the degradation. As shown in Fig. 14, the complete degradation of DCF (100%) was achieved without scavenger within 50 min of xenon light irradiation. In this work, para-benzoquinone (BQ), methanol, and tetra-butyl alcohol (TBA) were used as the scavengers for trapping the active species $^{\bullet}O_2^-$, h^+, and $^{\bullet}OH$, respectively. By adding 10 mmol L^{-1} of BQ to the suspension containing DCF and the optimal amount of the catalyst, the degradation percentage decreased to 18.6% after 50 min of xenon light irradiation. TBA and methanol (10 mmol L^{-1}) were added separately to the suspension containing DCF and the optimal amount of the synthesized catalyst. The degradation percentage reached 65% and 82.4% under xenon light irradiation, respectively. In addition, light absorption ability, separation efficiency, and lifetime of the charge carriers are also important factors in the photoactivity of a photocatalyst under visible light irradiation. TBA was an effective scavenger for $^{\bullet}OH$ and the observed stronger inhibition by TBA was probably due to the high viscosity of TBA that could mask the active sites on the bonding sites dispersed in the surface of the G/C-doped TiO_2 (Huang

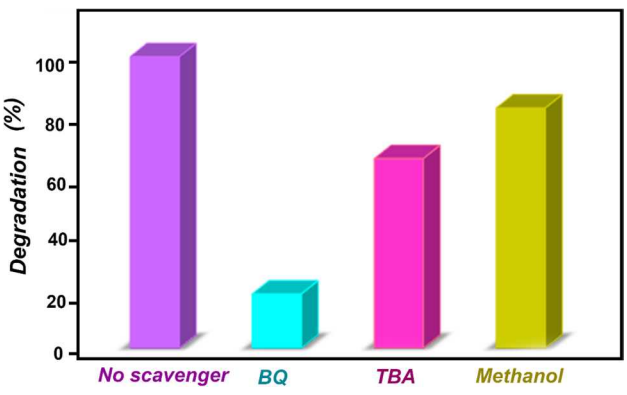

Fig.14 Scavenger (10 mmol L^{-1}) analysis on photocatalytic degradation of G/C-doped TiO_2 nanocomposite (C_0: 10 mg L^{-1}, photocatalyst: 0.05 g, xenon light duration: 50 min)

et al. 2017). Methanol is a known h^+_{vb} scavenger as well as an efficient scavenger of free or adsorbed •OH radicals. This result suggested that DCF was being photo-oxidized by direct interaction with the valence-band hole or by reaction with •OH radicals. Increases in the methanol concentration increased the competition for the oxidizing species, decreasing the degradation rate of DCF. It was found that the presence of methanol led to a significant inhibition in the rate of degradation of DCF due to the competition for •OH in the bulk medium. By adding the scavenger TBA and methanol with a specific concentration, the role of active hydroxyl radical and h^+ species in pollutant degradation was determined. Therefore, based on Fig. 14 and comparing the percentage of degradation, it is concluded that the active species are responsible for degradation and play a very important role in a photocatalytic reaction. It is also confirmed that in this photocatalytic experiment, $^{\bullet}O_2^-$ radicals played the main role in DCF degradation, and the role of active h^+ and •OH species in the degradation of DCF was less.

Based on the obtained results, a mechanism for DCF degradation under xenon light irradiation is proposed schematically in Fig. 15. By introducing carbon impurity into the TiO_2 lattice, novel impurity levels were created between the valance and the conduction layers of TiO_2. The impurity levels were formed through C_{1s} and a combination of the atomic orbitals of O_{2p} and C_{2p} (O_{2p}–C_{2p}) (Wang et al. 2012a; Jia et al. 2016). As the TiO_2 pure synthesized has a wide band gap (2.97 eV), it is not able to be active in the visible region and has little photocatalytic activity in the degradation of pollutants. Therefore, by introducing an impurity such as carbon, it is possible to narrow the band gap of TiO_2 and by shifting the absorption threshold to the visible area, improving its photocatalytic performance. In the case of the synthesized composite, it can be suggested that by exciting the TiO_2 with an energy higher than the band gap, the excited electrons in the valence band migrate to the new impurity level created by combining the orbits. In addition, by hybridizing the 2p orbitals of carbon and 2p oxygen, the electrons excited by light can be driven to the conductive band. Furthermore, by creating new impurity levels, photoexcited electrons can be increased from the level created by the hybridization of O_{2p} and C_{2p} atomic orbitals to the C_{1s} impurity level. By directing the electrons to the conduction band and the presence of new impurity levels, effective charge separation occurs and prevents hole-electron recombination. In addition, the excited electrons can be transferred to the graphite. By performing this operation, an effective separation occurs between the produced photoinduced electrons and holes and affects the performance of TiO_2 in the destruction of the desired pollutant (Jia et al. 2016; Eddy et al. 2023). In conclusion, the charge carriers produced by light induction were able to participate effectively in the photocatalytic reactions. Therefore, higher photocatalytic performance was observed in nanocomposite in comparison with TiO_2 as a pure compound.

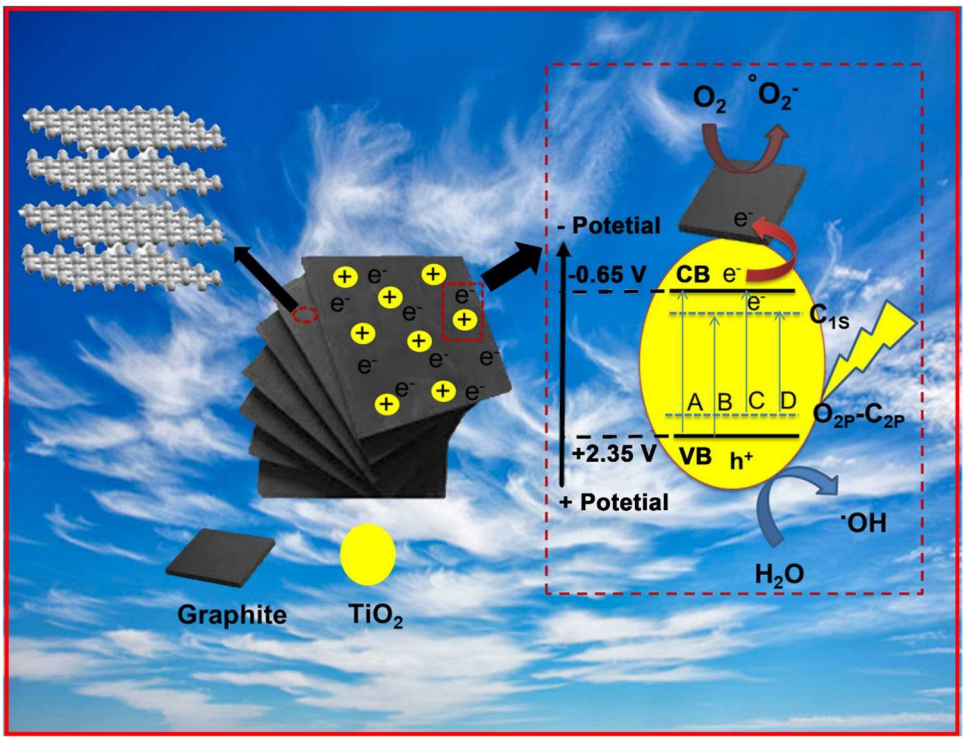

Fig. 15 Possible photo-catalytic mechanism of G/C-doped TiO_2 nanocomposite

Conclusion

A new G/C-doped TiO_2 nanophotocatalyst was synthesized successfully by ultrasound in a short time and at low temperatures. The use of ultrasound for material synthesis has been extensively increased in recent years. This method is not just a simple mixing tool. One of the current limitations of sonochemistry is related to the reproducibility of the process. The overall energy consumption of a sonochemical process is essential and the rate of sonochemical reactions completely depends on ultrasonic frequency. The development of sonochemical application on a larger scale is now a crucial challenge for sonochemists to reproduce the exciting results obtained in the lab into continuous or large-scale processes. Therefore, the combination of ultrasound with other innovative technologies starts to bring some interesting synergetic effects. The synergies brought by these combinations open the door to many new applications in green chemistry where the contribution of ultrasound becomes essential, although many studies on the larger-scale development of these combined technologies will be necessary. The complete degradation of DCF was achieved by this novel nanophotocatalyst under xenon light irradiation. Of all the nanophotocatalysts, the G/TiO_2 ratio with 0.03 g of G shows the highest photocatalytic activity in DCF degradation rate than the other mass in different ratios of G/TiO_2 under xenon light irradiation. The highest photocatalytic efficiency in a specific ratio of G/TiO_2 is closely related to the morphology, structure of the catalyst, vigorous light absorption, and narrow band gap. UV-DRS revealed that the synthesized G/C-doped TiO_2 nanoparticles exhibited absorption in the visible range of the electromagnetic spectrum. The results showed that there was a remarkable reduction in band gap from 2.97 to 2.75 eV for TiO_2 doped with carbon. The surface areas were increased significantly with the addition of graphite compared with TiO_2 and results reveal that the G-0.03 g sample shows higher surface areas than pure TiO_2. The XPS analysis confirmed that the doping and substituted carbon into the TiO_2 lattice can advance the segregation of photoinduced charge and diminish the band gap. The studies on different scavengers show that the $^{\bullet}O_2^-$ radical was the main reactive species in DCF degradation in comparison with the other active species. G (0.03 g)/C-doped TiO_2 composite showed high structural stability and reusability after consecutive runs. It is expected that the research conducted will furnish a novel and simple technique for the extensive synthesis of TiO_2-based photocatalysts, which will be widely used for non-selective anti-inflammatory drug contamination such as DFC.

Acknowledgements The support of Ferdowsi University of Mashhad (Research and Technology) is appreciated for this work (3/48842).

Author contribution Mohammad Barjasteh Moghaddam Roshtkhari: all experiments, analysis, and interpretation of results, conceptualization, methodology, investigation, formal analysis, and writing—original draft (first author). Mohammad Hassan Entezari: supervision, conceptualization, review, and editing (corresponding author).

Funding Ferdowsi University of Mashhad.

Data availability All data generated or analyzed during this study are included in this manuscript.

Declarations

Ethical approval Hereby, the authors consciously assure that for the manuscript "Graphite/C-doped TiO_2 nanocomposite synthesized by ultrasound for the degradation of DCF" the following is fulfilled: This manuscript is the author's original work, which has not been previously published elsewhere. The paper is not currently being considered for publication elsewhere and reflects the authors' research and analysis truthfully and completely.

Consent to participate Not applicable.

Consent for publication Not applicable.

Competing interests The authors declare no competing interests.

References

Adyani SM, Ghorbani M (2018) A comparative study of physicochemical and photocatalytic properties of visible light responsive Fe, Gd, and P single and tri-doped TiO_2 nanomaterials. J Rare Earths 36:72–85. https://doi.org/10.1016/j.jre.2017.06.012

Aghababaei N, Abdouss M, Hosseini-Monfared H, Ghanbari F (2023a) Enhanced photo-degradation of diclofenac using a new and effective composite (O-g-C_3N_4/TiO_2/α-Fe_2O_3): degradation pathway, toxicity evaluation and application for real matrix. J Environ Chem Eng 11:110477. https://doi.org/10.1016/j.jece.2023.110477

Aghababaei N, Abdouss M, Hosseini-Monfared H, Ghanbari F (2023b) Photocatalytic degradation of diclofenac using a novel double Z-scheme catalyst (O-g-C_3N_4/ZnO/TiO_2@halloysite nanotubes): degradation mechanism, identification of by-products and environmental implementation. J Water Process Eng 53. https://doi.org/10.1016/j.jwpe.2023.103702

Amalraj Appavoo I, Hu J, Huang Y et al (2014) Response surface modeling of carbamazepine (CBZ) removal by graphene-P25 nanocomposites/UVA process using central composite design. Water Res 57:270–279. https://doi.org/10.1016/j.watres.2014.03.007

Arai H, Arai M, Sakumoto A (1986) Exhaustive degradation of humic acid in water by simultaneous application of radiation and ozone. Water Res 20:885–891. https://doi.org/10.1016/0043-1354(86)90177-6

Baek M-H, Jung W-C, Yoon J-W et al (2013) Preparation, characterization and photocatalytic activity evaluation of micro- and mesoporous TiO_2/spherical activated carbon. J Ind Eng Chem 19:469–477. https://doi.org/10.1016/j.jiec.2012.08.026

Bang JH, Suslick KS (2010) Applications of ultrasound to the synthesis of nanostructured materials. Adv Mater 22:1039–1059. https://doi.org/10.1002/adma.200904093

Bhadra BN, Ahmed I, Kim S, Jhung SH (2016a) Adsorptive removal of ibuprofen and diclofenac from water using metal-organic

framework-derived porous carbon. Chem Eng J. https://doi.org/10.1016/j.cej.2016.12.127
Bhadra BN, Seo PW, Jhung SH (2016b) Adsorption of diclofenac sodium from water using oxidized activated carbon. Chem Eng J 301:27–34. https://doi.org/10.1016/j.cej.2016.04.143
Binas V, Venieri D, Kotzias D, Kiriakidis G (2017) Modified TiO_2 based photocatalysts for improved air and health quality. J Mater 3:3–16. https://doi.org/10.1016/j.jmat.2016.11.002
Boukhatem H, Khalaf H, Djouadi L et al (2017) Journal of Environmental Chemical Engineering under NUV – Vis irradiation . Operational parameters, kinetics and mechanism. 5:5636–5644. https://doi.org/10.1016/j.jece.2017.10.054
Byranvand MM, Kharat AN, Fatholahi L, Beiranvand ZM (2013) A review on synthesis of nano-TiO_2 via different methods. J Nanostruct 3:1–9. https://doi.org/10.7508/JNS.2013.01.001
Chen Q, Liu H, Xin Y, Cheng X (2013) TiO_2 nanobelts – Effect of calcination temperature on optical, photoelectrochemical and photocatalytic properties. Electrochim Acta 111:284–291. https://doi.org/10.1016/j.electacta.2013.08.049
Cheng X, Yu X, Xing Z (2012) Characterization and mechanism analysis of Mo–N-co-doped TiO_2 nano-photocatalyst and its enhanced visible activity. J Colloid Interface Sci 372:1–5. https://doi.org/10.1016/j.jcis.2011.11.071
Cheng X, Liu H, Chen Q et al (2013) Preparation and characterization of palladium nano-crystallite decorated TiO_2 nano-tubes photoelectrode and its enhanced photocatalytic efficiency for degradation of diclofenac. J Hazard Mater 254–255:141–148. https://doi.org/10.1016/j.jhazmat.2013.03.062
Colmenares QJC (2013) Ultrasound and photochemical procedures for nanocatalysts preparation: application in photocatalytic biomass valorization. J Nanosci Nanotechnol 13:4787–4798. https://doi.org/10.1166/jnn.2013.7567
Colmenares JC, Aramendía MA, Marinas A et al (2006) Synthesis, characterization and photocatalytic activity of different metal-doped titania systems. Appl Catal A Gen 306:120–127. https://doi.org/10.1016/j.apcata.2006.03.046
Coulter JB, Birnie DP (2018) Assessing Tauc plot slope quantification: ZnO thin films as a model system. Phys Status Solidi Basic Res 255:1–7. https://doi.org/10.1002/pssb.201700393
Di Credico B, Bellobono IR, D'Arienzo M et al (2015) Efficacy of the reactive oxygen species generated by immobilized TiO_2 in the photocatalytic degradation of diclofenac. Int J Photoenergy 2015. https://doi.org/10.1155/2015/919217
da Silva AL, Trindade FJ, Lou DJ et al (2022) Synthesis of TiO_2 microspheres by ultrasonic spray pyrolysis and photocatalytic activity evaluation. Ceram Int 48:9739–9745. https://doi.org/10.1016/j.ceramint.2021.12.175
De Luis AM, Lombraña JI, Menéndez A, Sanz J (2011) Analysis of the toxicity of phenol solutions treated with H_2O_2/UV and H_2O_2/Fe oxidative systems. Ind Eng Chem Res 50:1928–1937. https://doi.org/10.1021/ie101435u
Di Valentin C, Pacchioni G, Selloni A (2005) Theory of carbon doping of titanium dioxide. Chem Mater 17:6656–6665. https://doi.org/10.1021/cm051921h
Di J, Li S, Zhao Z et al (2015) Biomimetic CNT@TiO_2 composite with enhanced photocatalytic properties. Chem Eng J 281:60–68. https://doi.org/10.1016/j.cej.2015.06.067
Djellabi R, Yang B, Wang Y et al (2019a) Carbonaceous biomass-titania composites with Ti–O–C bonding bridge for efficient photocatalytic reduction of Cr(VI) under narrow visible light. Chem Eng J 366:172–180. https://doi.org/10.1016/j.cej.2019.02.035
Djellabi R, Yang B, Xiao K et al (2019b) Unravelling the mechanistic role of Ti–O–C bonding bridge at titania/lignocellulosic biomass interface for Cr(VI) photoreduction under visible light. J Colloid Interface Sci 553:409–417. https://doi.org/10.1016/j.jcis.2019.06.052
Dong X, Sun Z, Zhang X et al (2018) Synthesis and enhanced solar light photocatalytic activity of a C/N Co-doped TiO_2/diatomite composite with exposed (001) facets. Aust J Chem 71:315–324. https://doi.org/10.1071/CH17544
Eddy DR, Permana MD, Sakti LK et al (2023) Heterophase polymorph of TiO_2 (anatase, rutile, brookite, TiO_2 (B)) for efficient photocatalyst: fabrication and activity. Nanomaterials 13. https://doi.org/10.3390/nano13040704
Etacheri V, Michlits G, Seery MK et al (2013) A highly efficient $TiO_{2-x}C_x$ nano-heterojunction photocatalyst for visible light induced antibacterial applications. ACS Appl Mater Interfaces 5:1663–1672. https://doi.org/10.1021/am302676a
Fabbri D, López-Muñoz MJ, Daniele A et al (2019) Photocatalytic abatement of emerging pollutants in pure water and wastewater effluent by TiO_2 and Ce-ZnO: degradation kinetics and assessment of transformation products. Photochem Photobiol Sci 18:845–852. https://doi.org/10.1039/c8pp00311d
Gao P, Li A, Sun DD, Ng WJ (2014) Effects of various TiO_2 nanostructures and graphene oxide on photocatalytic activity of TiO_2. J Hazard Mater 279:96–104. https://doi.org/10.1016/j.jhazmat.2014.06.061
García-Araya JF, Beltrán FJ, Aguinaco A (2010) Diclofenac removal from water by ozone and photolytic TiO_2 catalysed processes. J Chem Technol Biotechnol 85:798–804. https://doi.org/10.1002/jctb.2363
Gil A, García AM, Fernández M et al (2017) Effect of dopants on the structure of titanium oxide used as a photocatalyst for the removal of emergent contaminants. J Ind Eng Chem 53:183–191. https://doi.org/10.1016/j.jiec.2017.04.024
González-Reyes L, Hernández-Pérez I, Díaz-Barriga Arceo L et al (2010) Temperature effects during Ostwald ripening on structural and bandgap properties of TiO_2 nanoparticles prepared by sonochemical synthesis. Mater Sci Eng B 175:9–13. https://doi.org/10.1016/j.mseb.2010.06.004
Güler Ö, Güler SH, Selen V et al (2016) Production of graphene layer by liquid-phase exfoliation with low sonication power and sonication time from synthesized expanded graphite. Fuller Nanotub Carbon Nanostructures 24:123–127. https://doi.org/10.1080/1536383X.2015.1114472
Gümüş D, Akbal F (2011) Photocatalytic degradation of textile dye and wastewater. Water, Air, Soil Pollut 216:117–124. https://doi.org/10.1007/s11270-010-0520-z
He Z, Que W, He Y (2014) Enhanced photocatalytic performance of sensitized mesoporous TiO_2 nanoparticles by carbon mesostructures. RSC Adv 4:3332–3339. https://doi.org/10.1039/C3RA46389C
Huang Q, Tian S, Zeng D et al (2013a) Enhanced photocatalytic activity of chemically bonded TiO_2 /graphene composites based on the effective interfacial charge transfer through the C-Ti bond. ACS Catal 3:1477–1485. https://doi.org/10.1021/cs400080w
Huang T, Mao S, Yu J et al (2013b) Effects of N and F doping on structure and photocatalytic properties of anatase TiO_2 nanoparticles. RSC Adv 3:16657. https://doi.org/10.1039/c3ra42600a
Huang X, Wang L, Zhou J, Gao N (2014) Photocatalytic decomposition of bromate ion by the UV/P25-graphene processes. Water Res 57:1–7. https://doi.org/10.1016/j.watres.2014.02.042
Huang GX, Wang CY, Yang CW et al (2017) Degradation of bisphenol a by peroxymonosulfate catalytically activated with Mn1.8Fe1.2O4 nanospheres: synergism between Mn and Fe. Environ Sci Technol 51:12611–12618. https://doi.org/10.1021/acs.est.7b03007

In S, Kean AH, Orlov A et al (2009) A versatile new method for synthesis and deposition of doped, visible light-activated TiO_2 thin films. Energy Environ Sci 2:1277. https://doi.org/10.1039/b915060a

Inagaki M (2012) Carbon coating for enhancing the functionalities of materials. Carbon N Y 50:3247–3266. https://doi.org/10.1016/j.carbon.2011.11.045

Jia J, Li D, Wan J, Yu X (2016) Characterization and mechanism analysis of graphite/C-doped TiO_2 composite for enhanced photocatalytic performance. J Ind Eng Chem 33:162–169. https://doi.org/10.1016/j.jiec.2015.09.030

Keen OS, Thurman EM, Ferrer I et al (2013) Dimer formation during UV photolysis of diclofenac. Chemosphere 93:1948–1956. https://doi.org/10.1016/j.chemosphere.2013.06.079

Khetan SK, Collins TJ (2007) Human pharmaceuticals in the aquatic environment: a challenge to green chemisty. Chem Rev 107:2319–2364. https://doi.org/10.1021/cr020441w

Kim K (1990) Structure and composition requirements for deoxygenation, dehydration, and ketonization reactions of carboxylic acids on TiO_2(001) single-crystal surfaces. J Catal 125:353–375. https://doi.org/10.1016/0021-9517(90)90309-8

Kohtani S, Kudo A, Sakata T (1993) Spectral sensitization of a TiO_2 semiconductor electrode by CdS microcrystals and its photoelectrochemical properties. Chem Phys Lett 206:166–170. https://doi.org/10.1016/0009-2614(93)85535-V

Kongkanand A, Kama PV (2007) Electron storage in single wall carbon semiconductor – SWCNT suspensions. ACS Nano 1:13–21. https://doi.org/10.1021/nn700036f

Kumar A (2018) Different methods used for the synthesis of TiO_2 based nanomaterials: a review. Am J Nano Res Appl 6:1. https://doi.org/10.11648/j.nano.20180601.11

Lara-Pérez C, Leyva E, Zermeño B et al (2020) Photocatalytic degradation of diclofenac sodium salt: adsorption and reaction kinetic studies. Environ Earth Sci 79:1–13. https://doi.org/10.1007/s12665-020-09017-z

Lee S, Lee Y, Kim DH, Moon JH (2013) Carbon-deposited TiO_2 3D inverse opal photocatalysts: visible-light photocatalytic activity and enhanced activity in a viscous solution. ACS Appl Mater Interfaces 5:12526–12532. https://doi.org/10.1021/am403820e

Li G, Li L, Boerio-Goates J, Woodfield BF (2005) High purity anatase TiO_2 nanocrystals: near room-temperature synthesis, grain growth kinetics, and surface hydration chemistry. J Am Chem Soc 127:8659–8666. https://doi.org/10.1021/ja050517g

Li D, Cheng X, Yu X, Xing Z (2015a) Preparation and characterization of TiO_2 -based nanosheets for photocatalytic degradation of acetylsalicylic acid: Influence of calcination temperature. Chem Eng J 279:994–1003. https://doi.org/10.1016/j.cej.2015.05.102

Li D, Xing Z, Yu X, Cheng X (2015b) One-step hydrothermal synthesis of C-N-S-tridoped TiO_2-based nanosheets photoelectrode for enhanced photoelectrocatalytic performance and mechanism. Electrochim Acta 170:182–190. https://doi.org/10.1016/j.electacta.2015.04.148

Li D, Jia J, Zhang Y et al (2016a) Preparation and characterization of nano-graphite/TiO_2 composite photoelectrode for photoelectrocatalytic degradation of hazardous pollutant. J Hazard Mater 315:1–10. https://doi.org/10.1016/j.jhazmat.2016.04.053

Li J, Xu X, Liu X et al (2016b) Sn doped TiO_2 nanotube with oxygen vacancy for highly efficient visible light photocatalysis. J Alloys Compd 679:454–462. https://doi.org/10.1016/j.jallcom.2016.04.080

Li Q, Guan Z, Wu D et al (2017) Z-scheme BiOCl-Au-CdS heterostructure with enhanced sunlight-driven photocatalytic activity in degrading water dyes and antibiotics. ACS Sustain Chem Eng 5:6958–6968. https://doi.org/10.1021/acssuschemeng.7b01157

Li J, Pham AN, Dai R et al (2020a) Recent advances in Cu-Fenton systems for the treatment of industrial wastewaters: role of Cu complexes and Cu composites. J Hazard Mater 392:122261. https://doi.org/10.1016/j.jhazmat.2020.122261

Li W, Liang R, Zhou NY, Pan Z (2020b) Carbon black-doped anatase TiO_2 nanorods for solar light-induced photocatalytic degradation of methylene blue. ACS Omega 5:10042–10051. https://doi.org/10.1021/acsomega.0c00504

Liu L, Chen X (2014) Titanium dioxide nanomaterials: self-structural modifications. Chem Rev 114:9890–9918. https://doi.org/10.1021/cr400624r

Liu R, Li W (2018) High-thermal-stability and high-thermal-conductivity $Ti_3C_2T_x$ MXene/poly(vinyl alcohol) (PVA) composites. ACS Omega 3:2609–2617. https://doi.org/10.1021/acsomega.7b02001

Liu G, Han C, Pelaez M et al (2013) Enhanced visible light photocatalytic activity of CN-codoped TiO_2 films for the degradation of microcystin-LR. J Mol Catal A Chem 372:58–65. https://doi.org/10.1016/j.molcata.2013.02.006

Liu W, Li Y, Liu F et al (2019) Visible-light-driven photocatalytic degradation of diclofenac by carbon quantum dots modified porous g-C3N4: mechanisms, degradation pathway and DFT calculation. Water Res 151:8–19. https://doi.org/10.1016/j.watres.2018.11.084

Makal P, Das D (2018) Self-doped TiO_2 nanowires in TiO_2 -B single phase, TiO_2 -B/anatase and TiO_2 -anatase/rutile heterojunctions demonstrating individual superiority in photocatalytic activity under visible and UV light. Appl Surf Sci 455:1106–1115. https://doi.org/10.1016/j.apsusc.2018.06.055

Malato S, Fernández-Ibáñez P, Maldonado MI et al (2009) Decontamination and disinfection of water by solar photocatalysis: recent overview and trends. Catal Today 147:1–59. https://doi.org/10.1016/j.cattod.2009.06.018

Mali SS, Betty CA, Bhosale PN, Patil PS (2012) Synthesis, characterization of hydrothermally grown MWCNT–TiO_2 photoelectrodes and their visible light absorption properties. ECS J Solid State Sci Technol 1:M15–M23. https://doi.org/10.1149/2.004202jss

Mason TJ (2003) Sonochemistry and sonoprocessing: the link, the trends and (probably) the future. Ultrason Sonochem 10:175–179. https://doi.org/10.1016/S1350-4177(03)00086-5

McDevitt NT, Baun WL (1964) Infrared absorption study of metal oxides in the low frequency region (700–240 cm^{-1}). Spectrochim Acta 20:799–808. https://doi.org/10.1016/0371-1951(64)80079-5

Mergbi M, Aboagye D, Contreras S et al (2023) Fast g-C_3N_4 sono-coated activated carbon for enhanced solar photocatalytic oxidation of organic pollutants through Adsorb & Shuttle process. Ultrason Sonochem 99:106550. https://doi.org/10.1016/j.ultsonch.2023.106550

Meroni D, Djellabi R, Ashokkumar M et al (2022) Sonoprocessing : from concepts to large-scale reactors. Chem Rev 122:3219–3258. https://doi.org/10.1021/acs.chemrev.1c00438

Michael I, Achilleos A, Lambropoulou D et al (2014) Proposed transformation pathway and evolution profile of diclofenac and ibuprofen transformation products during (sono)photocatalysis. Appl Catal B Environ 147:1015–1027. https://doi.org/10.1016/j.apcatb.2013.10.035

Moctezuma E, Leyva E, Lara-Pérez C et al (2020) TiO_2 photocatalytic degradation of diclofenac: intermediates and total reaction mechanism. Top Catal 63:601–615. https://doi.org/10.1007/s11244-020-01262-7

Mohamed RM, Mkhalid IA (2015) Visible light photocatalytic degradation of cyanide using Au-TiO_2/multi-walled carbon nanotube nanocomposites. J Ind Eng Chem 22:390–395. https://doi.org/10.1016/j.jiec.2014.07.037

Mortazavi S, NorouziFard PSA (2017) Quantitative Assessment of Concentration of Pharmaceutical Pollutants (Naproxen, Diclofenac, and Celecoxib) in the Karaj River, Alborz Province, Iran. J Rafsanjan Univ Med Sci 16:605–622

Neville EM, Mattle MJ, Loughrey D et al (2012) Carbon-doped TiO_2 and carbon, tungsten-codoped TiO_2 through Sol-Gel processes in the presence of melamine borate: reflections through photocatalysis. J Phys Chem C 116:16511–16521. https://doi.org/10.1021/jp303645p

Nguyen NT, Nguyen VA (2020) Synthesis, characterization, and photocatalytic activity of ZnO nanomaterials prepared by a green, nonchemical route. J Nanomater 2020:1–8. https://doi.org/10.1155/2020/1768371

Ojeda M, Chen B, Leung DYC et al (2017) A hydrogel template synthesis of TiO_2 nanoparticles for aluminium-ion batteries. Energy Procedia 105:3997–4002. https://doi.org/10.1016/j.egypro.2017.03.836

Ong W-J, Tan L-L, Chai S-P et al (2014) Highly reactive 001 facets of TiO2-based composites: synthesis, view article online 10.1039/C3NR04655A Formation mechanism and characterizations. Nanoscale 6:1946–2008. https://doi.org/10.1039/C3NR04655A.This

Palmisano G, Loddo V, El NHH et al (2009) Graphite-supported TiO_2 for 4-nitrophenol degradation in a photoelectrocatalytic reactor. Chem Eng J 155:339–346. https://doi.org/10.1016/j.cej.2009.07.002

Panjiar H, Gakkhar RP, Daniel BSS (2015) Strain-free graphite nanoparticle synthesis by mechanical milling. Powder Technol 275:25–29. https://doi.org/10.1016/j.powtec.2015.01.056

Prahas D, Kartika Y, Indraswati N, Ismadji S (2008) Activated carbon from jackfruit peel waste by H_3PO_4 chemical activation: pore structure and surface chemistry characterization. Chem Eng J 140:32–42. https://doi.org/10.1016/j.cej.2007.08.032

Qamar M, Muneer M (2009) A comparative photocatalytic activity of titanium dioxide and zinc oxide by investigating the degradation of vanillin. Desalination 249:535–540. https://doi.org/10.1016/j.desal.2009.01.022

Rajeshkumar R, Udhayabanu V, Srinivasan A, Ravi KR (2017) Microstructural evolution in ultrafine grained Al-graphite composite synthesized via combined use of ultrasonic treatment and friction stir processing. J Alloys Compd 726:358–366. https://doi.org/10.1016/j.jallcom.2017.07.280

Rashid J, Karim S, Kumar R et al (2020) A facile synthesis of bismuth oxychloride-graphene oxide composite for visible light photocatalysis of aqueous diclofenac sodium. Sci Rep 10:1–11. https://doi.org/10.1038/s41598-020-71139-y

Rey A, Mena E, Chávez AM et al (2015) Influence of structural properties on the activity of WO_3 catalysts for visible light photocatalytic ozonation. Chem Eng Sci 126:80–90. https://doi.org/10.1016/j.ces.2014.12.016

Rozman D, Hrkal Z, Eckhardt P et al (2015) Pharmaceuticals in groundwaters: a case study of the psychiatric hospital at Horní Beřkovice, Czech Republic. Environ Earth Sci 73:3775–3784. https://doi.org/10.1007/s12665-014-3663-1

Safarifard V, Morsali A (2012) Sonochemical syntheses of a nanosized copper(II) supramolecule as a precursor for the synthesis of copper(II) oxide nanoparticles. Ultrason Sonochem 19:823–829. https://doi.org/10.1016/j.ultsonch.2011.12.013

Salaeh S, Juretic Perisic D, Biosic M et al (2016) Diclofenac removal by simulated solar assisted photocatalysis using TiO_2-based zeolite catalyst; mechanisms, pathways and environmental aspects. Chem Eng J 304:289–302. https://doi.org/10.1016/j.cej.2016.06.083

Sander JRG, Zeiger BW, Suslick KS (2014) Sonocrystallization and sonofragmentation. Ultrason Sonochem 21:1908–1915. https://doi.org/10.1016/j.ultsonch.2014.02.005

Sathishkumar P, Mohan K, Meena RAA et al (2021) Hazardous impact of diclofenac on mammalian system: Mitigation strategy through green remediation approach. J Hazard Mater 419:126135. https://doi.org/10.1016/j.jhazmat.2021.126135

Schulze-Hennings U, Brückner I, Gebhardt W et al (2017) Durability of a coating containing titanium dioxide for the photocatalytic degradation of diclofenac in water with UV-A irradiation. Water Environ J 31:508–514. https://doi.org/10.1111/wej.12272

Shchukin DG, Skorb E, Belova V, Möhwald H (2011) Ultrasonic cavitation at solid surfaces. Adv Mater 23:1922–1934. https://doi.org/10.1002/adma.201004494

Shen J, Yan B, Shi M et al (2011a) One step hydrothermal synthesis of TiO_2-reduced graphene oxide sheets. J Mater Chem 21:3415. https://doi.org/10.1039/c0jm03542d

Shen Y, Zhou P, Sun QQ et al (2011b) Optical investigation of reduced graphene oxide by spectroscopic ellipsometry and the band-gap tuning. Appl Phys Lett 99:2011–2014. https://doi.org/10.1063/1.3646908

Sibu CP, Kumar SR, Mukundan P, Warrier KGK (2002) Structural modifications and associated properties of lanthanum oxide doped sol−gel nanosized titanium oxide. Chem Mater 14:2876–2881. https://doi.org/10.1021/cm010966p

Tauc J, Grigorovici R, Vancu A (1966) Optical properties and electronic structure of amorphous germanium. Phys Status Solidi 15:627–637. https://doi.org/10.1002/pssb.19660150224

Teh CY, Wu TY, Juan JC (2015) Facile sonochemical synthesis of N, Cl-codoped Ti_O2: synthesis effects, mechanism and photocatalytic performance. Catal Today 256:365–374. https://doi.org/10.1016/j.cattod.2015.02.014

Thomas RT, Abdul Rasheed P, Sandhyarani N (2014) Synthesis of nanotitania decorated few-layer graphene for enhanced visible light driven photocatalysis. J Colloid Interface Sci 428:214–221. https://doi.org/10.1016/j.jcis.2014.04.054

Tiple A, Sinhmar PS, Gogate PR (2021) Improved direct synthesis of TiO_2 catalyst using sonication and its application for the desulfurization of thiophene. Ultrason Sonochem 73:105547. https://doi.org/10.1016/j.ultsonch.2021.105547

Tseng WJ, Chao P-S (2013) Synthesis and photocatalysis of TiO_2 hollow spheres by a facile template-implantation route. Ceram Int 39:3779–3787. https://doi.org/10.1016/j.ceramint.2012.10.217

Ullah K, Da MZ, Ye S et al (2014) Synthesis and characterization of novel PbS-graphene/TiO_2 composite with enhanced photocatalytic activity. J Ind Eng Chem 20:1035–1042. https://doi.org/10.1016/j.jiec.2013.06.040

Velempini T, Prabakaran E, Pillay K (2021) Recent developments in the use of metal oxides for photocatalytic degradation of pharmaceutical pollutants in water—a review. Mater Today Chem 19:100380. https://doi.org/10.1016/j.mtchem.2020.100380

Wang Y, Shi R, Lin J, Zhu Y (2010) Significant photocatalytic enhancement in methylene blue degradation of TiO_2 photocatalysts via graphene-like carbon in situ hybridization. Appl Catal B Environ 100:179–183. https://doi.org/10.1016/j.apcatb.2010.07.028

Wang DH, Jia L, Wu XL et al (2012a) One-step hydrothermal synthesis of N-doped TiO_2/C nanocomposites with high visible light photocatalytic activity. Nanoscale 4:576–584. https://doi.org/10.1039/c1nr11353d

Wang X-K, Wang C, Zhang D (2012b) Sonochemical synthesis and characterization of Cl–N-codoped TiO_2 nanocrystallites. Mater Lett 72:12–14. https://doi.org/10.1016/j.matlet.2011.12.067

Wang Y, Wang Q, Zhan X et al (2013) Visible light driven type II heterostructures and their enhanced photocatalysis properties: a review. Nanoscale 5:8326–8339. https://doi.org/10.1039/c3nr01577g

Woan K, Pyrgiotakis G, Sigmund W (2009) Photocatalytic carbon-nanotube-TiO_2 composites. Adv Mater 21:2233–2239. https://doi.org/10.1002/adma.200802738

Xu Z, Yu J (2011) Visible-light-induced photoelectrochemical behaviors of Fe-modified TiO_2 nanotube arrays. Nanoscale 3:3138. https://doi.org/10.1039/c1nr10282f

Yang X, Cao C, Erickson L et al (2009) Photo-catalytic degradation of Rhodamine B on C-, S-, N-, and Fe-doped TiO_2 under visible-light irradiation. Appl Catal B Environ 91:657–662. https://doi.org/10.1016/j.apcatb.2009.07.006

Yi C, Liao Q, Deng W et al (2019) The preparation of amorphous TiO_2 doped with cationic S and its application to the degradation of DCFs under visible light irradiation. Sci Total Environ 684:527–536. https://doi.org/10.1016/j.scitotenv.2019.05.338

Yu J, Dai G, Xiang Q, Jaroniec M (2011) Fabrication and enhanced visible-light photocatalytic activity of carbon self-doped TiO2 sheets with exposed 001 facets. J Mater Chem 21:1049–1057. https://doi.org/10.1039/C0JM02217A

Yu J, Li Q, Liu S, Jaroniec M (2013) Ionic-liquid-assisted synthesis of uniform fluorinated B/C-codoped TiO_2 nanocrystals and their enhanced visible-light photocatalytic activity. Chem - A Eur J 19:2433–2441. https://doi.org/10.1002/chem.201202778

Yu X, Zhang Y, Cheng X (2014) Preparation and photoelectrochemical performance of expanded graphite/TiO_2 composite. Electrochim Acta 137:668–675. https://doi.org/10.1016/j.electacta.2014.06.027

Zaka A, Ibrahim TH, Khamis M (2021) Removal of selected non-steroidal anti-inflammatory drugs from wastewater using reduced graphene oxide magnetite. Desalin Water Treat 212:401–414. https://doi.org/10.5004/dwt.2021.26686

Zhang L-W, Fu H-B, Zhu Y-F (2008) Efficient TiO_2 photocatalysts from surface hybridization of TiO_2 particles with graphite-like carbon. Adv Funct Mater 18:2180–2189. https://doi.org/10.1002/adfm.200701478

Zhang G, Teng F, Wang Y et al (2013) Preparation of carbon-TiO_2 nanocomposites by a hydrothermal method and their enhanced photocatalytic activity. RSC Adv 3:24644–24649. https://doi.org/10.1039/c3ra44950e

Zhang G, Kim G, Choi W (2014a) Visible light driven photocatalysis mediated via ligand-to-metal charge transfer (LMCT): An alternative approach to solar activation of titania. Energy Environ Sci 7:954–966. https://doi.org/10.1039/c3ee43147a

Zhang Y, Zhou Z, Chen T et al (2014b) Graphene TiO_2 nanocomposites with high photocatalytic activity for the degradation of sodium pentachlorophenol. J Environ Sci 26:2114–2122. https://doi.org/10.1016/j.jes.2014.08.011

Zhang Y, Zhao Z, Chen J et al (2015a) C-doped hollow TiO_2 spheres: in situ synthesis, controlled shell thickness, and superior visible-light photocatalytic activity. Appl Catal B Environ 165:715–722. https://doi.org/10.1016/j.apcatb.2014.10.063

Zhou L, Wang W, Liu S et al (2006) A sonochemical route to visible-light-driven high-activity $BiVO_4$ photocatalyst. J Mol Catal A Chem 252:120–124. https://doi.org/10.1016/j.molcata.2006.01.052

Zhou W, Yu C, Fan Q et al (2013) Ultrasonic fabrication of N-doped TiO_2 nanocrystals with mesoporous structure and enhanced visible light photocatalytic activity. Cuihua Xuebao/chinese J Catal 34:1250–1255. https://doi.org/10.1016/S1872-2067(12)60578-6

Zhu M, Wang R, Chen C et al (2017) Electrochemical study on the corrosion behavior of Ti_3SiC_2 in 3.5% NaCl solution. RSC Adv 7:12534–12540. https://doi.org/10.1039/c6ra26239b

Zhu X, Zhou Q, Xia Y et al (2021) Preparation and characterization of Cu-doped TiO_2 nanomaterials with anatase/rutile/brookite triphasic structure and their photocatalytic activity. J Mater Sci Mater Electron 32:21511–21524. https://doi.org/10.1007/s10854-021-06660-5

Zhuang H-F, Lin C-J, Lai Y-K et al (2007) Some critical structure factors of titanium oxide nanotube array in its photocatalytic activity. Environ Sci Technol 41:4735–4740. https://doi.org/10.1021/es0702723